Late Quaternary mud-dominated, basin-floor sedimentation of the Gulf of Corinth, Greece: Implications for deep-water depositional processes and controls on syn-rift sedimentation

Rob L Gawthorpe, Natacha Fabregas, Sofia Pechlivanidou, Mary Ford, Richard E Ll Collier, Gareth D O Carter, Lisa C Mcneill, Donna J Shillington

Received: 28 October 2021 | Revised: 26 March 2022 | Accepted: 6 April 2022

DOI: 10.1111/bre.12671

Basin Research | IAS EAGE | WILEY

ORIGINAL RESEARCH

Late Quaternary mud-dominated, basin-floor sedimentation of the Gulf of Corinth, Greece: Implications for deep-water depositional processes and controls on syn-rift sedimentation

Rob L. Gawthorpe[1] | **Natacha Fabregas**[1] | **Sofia Pechlivanidou**[1] | **Mary Ford**[2] | **Richard E. Ll. Collier**[3] | **Gareth D. O. Carter**[4] | **Lisa C. McNeill**[5] | **Donna J. Shillington**[6]

[1]Department of Earth Science, University of Bergen, Bergen, Norway

[2]Université de Lorraine, CNRS, CRPG, Nancy, France

[3]School of Earth and Environment, University of Leeds, Leeds, UK

[4]British Geological Survey, The Lyell Centre, Edinburgh, UK

[5]Ocean and Earth Science, National Oceanography Centre Southampton, University of Southampton, Southampton, UK

[6]School of Earth and Sustainability, Northern Arizona University, Flagstaff, Arizona, USA

Correspondence
Rob L. Gawthorpe, Department of Earth Science, University of Bergen, P.O. Box 7803, 5020 Bergen, Norway.
Email: rob.gawthorpe@uib.no

Funding information
Norges Forskningsråd, Grant/Award: number 308805. Det Norske Videnskaps-Akademi, Grant/Award: VISTA Professorship. Natural Environmental Research Council, Grant/Award: NE/S002367/1

Abstract

Syn-rift deep-water muds and mudstones preserve a relatively complete stratigraphic record of tectonic and climatic events. This paper investigates mud-dominated deposits and stratigraphy using core from International Ocean Discovery Program (IODP) Expedition 381 sites M0078 and M0079 in the Gulf of Corinth, Greece. Millimetre-scale logging defined several bed types: homogeneous and laminated mud beds, bioturbated beds, a variety of graded beds, and rare matrix-supported conglomerates and slumps. Homogeneous muds and light grey to black laminated muds record deposition from distal, waning low density turbidity currents and terminal mud-rich quasi-laminar or laminar plug flows. Graded beds, interpreted as turbidites, range from beds several millimetre to a few centimetres of mud with silt to fine sand bases, to metre-scale mud beds with coarser sand and pebble bases. Conglomerate and slumped beds record cohesive debris flows, transitional flows and slope failure. Three stratal package types are distinguished: bioturbated, bedded and laminated, recording distinct hydrological conditions. Bioturbated packages record interglacial marine conditions with well oxygenated waters. Bedded packages record hemipelagic processes and low energy density underflows in a mainly dysoxic, stratified, lacustrine setting (glacial phases). In laminated packages, white mm-scale laminae of calcite or aragonite from varved, hemipelagic sediments demonstrating seasonal variability in a dysoxic non-marine or transitional setting. Rift stratigraphy is linked to eustatically controlled connections to the global ocean across rift segment boundaries. The ca. 780 to 330 ka succession is dominated by laminated packages with thin bioturbated packages and distinct conglomerates and slumps, suggesting high sills, making ocean connections brief and transitional to lacustrine conditions prolonged. The ca. 330 ka to present succession

shows well developed bioturbated and bedded packages, separated by thin laminated packages, suggesting brief transitions and well-developed marine conditions due to lower sills. Results indicate that structurally controlled rift segment boundaries exert a first-order control on syn-rift stratigraphic evolution, with fault segment growth and linkage driving intra-rift facies and sequence variability.

KEYWORDS

Gulf of Corinth, hemipelagites, IODP Expedition 381, mud, normal fault, Quaternary, rift, sea-level change, turbidites

1 | INTRODUCTION

The sedimentary record of continental rifts reflects the combination of driving tectonic and surface processes (e.g. Collier et al., 2000; Cowie et al., 2006; Gawthorpe & Leeder, 2000; Lyons et al., 2011; Pechlivanidou et al., 2019). To date syn-rift tectono-sedimentary and tectono-geomorphological studies have focused on coarse-grained basin margin successions such as transverse-fed alluvial fans and coarse-grained deltaic shorelines (e.g. Backert et al., 2010; Dorsey et al., 1997; Whittaker et al., 2010), basin margin turbidite fans (e.g. Cullen et al., 2021), and to a lesser extent axial fluvial systems (Alexander et al., 1994; Geurts et al., 2020). In contrast, syn-rift deep-water muds and mudstones, the dominant lithology in marine rift-axis depocentres, have received much less attention despite their potential to preserve a relatively full stratigraphic record of tectonic and climatic events.

Mud-dominated basinal sedimentation may arise from a range of disparate processes such as by settling out of suspension, by deposition from dilute, low-density turbidity currents distal to deltas and base-of-slope fans and slope failures, or by a range of debris flows and transitional flows which may evolve from slope failure events. The transport of mud as a component of turbulent underflows and its deposition by deceleration and distal run-out as the fine-grained end-member of turbidites has long been recognised (Bouma, 1962; Lowe, 1982; Mulder & Alexander, 2001). Experimental studies have led to the recognition that mud-bearing flows may transition between turbulent and laminar conditions by, for example, the addition of mud from the underlying substrate (Baas et al., 2009, 2011; Baas & Best, 2002). A variety of sedimentary structures may result from deposition out of waning, low-density distal turbidites including parallel-laminated or homogeneous muds, bipartite beds of sand overlain by silt/clay, current ripples, and normal grading. Unstructured, homogeneous muds may also record deposition in distal depositional lows by slow-moving and decelerating mud-rich flows in which non-Newtonian, laminar plug flow behaviour arises from mud being entrained into a distal turbidity current. Unstructured muds may result from this "freezing" of low velocity plug flows with low strength (and low Froude numbers), as inferred for example in the Marnoso Arenacea Formation, northern Italy (Talling et al., 2007).

The characteristics of mud-supported conglomerates are well established in the literature. An upward coarsening and upward increase in the concentration of clasts and blocks provides evidence of cohesive debris flow behaviour (Lowe, 1982; Mulder & Alexander, 2001; Talling, 2013), and the presence of laminated muds or very fine sands on the top of the debrite bed may indicate intermediate strength laminar cohesive debris flow behaviour in the late stages of deposition or the presence of a turbulent cloud produced by mixing (Talling, 2013). Intraclasts of laminated muds or fine sands are commonly folded and/or show extensional fractures, evidence of both plastic and brittle deformation of clasts within the flow. In the absence of intraclasts it may be difficult to distinguish a muddy debrite from a homogeneous hemipelagite accumulated by deposition of suspended particles from the

Highlights

- IODP 381 cores, Corinth Rift, Greece, reveal rift axis, mud-dominated deposits of the last 800 kyr.
- Sediments are homogeneous, laminated or bioturbated muds, graded beds, minor conglomerates and slumps, predominantly deposited by sediment gravity flows.
- Bedded and laminated mud packages record a stratified lake when eustatic sea-level was below structural sills.
- Marine bioturbated packages formed during eustatic highstands, with aragonitic varves at lacustrine-marine transitions.
- Tectonic control of sill height at rift segment boundaries is a major control on rift basin stratigraphy.

water column, and which may comprise a combination of fine-grained terrigenous material, planktonic organisms and windblown sediment. Characteristics of hemipelagites include a lack of sedimentary structures, preservation of non-fragmented fragile biogenic material, a lack of coarse grains and, in the case of clay-rich hemipelagites, disorganised clay fabrics (Ochoa et al., 2013).

Recent integrated studies combining microscopy with outcrop or core description have been used to explore the range of processes by which muds may be transported in deep-water settings (Ayranci et al., 2018; Konitzer et al., 2014; Newport et al., 2018; Schieber, 1999; Talling et al., 2007). Muds associated with basin-floor fans in relatively open settings (>100 km run-out), have been ascribed to a variety of gravity flow types and have been differentiated from hemipelagic suspension fall-out deposits (Boulesteix et al., 2019). However, there remains little work on the character and controls of mud deposition in rift depocentres which may have multiple lateral and axial clastic inputs and short run-out distances (in the order of 10 km).

The Corinth Rift offers a unique opportunity to investigate the range of mud-dominated deposits in syn-rift basinal depocentres using cores from the International Ocean Discovery Program (IODP) Expedition 381 (McNeill, Shillington, Carter, & Expedition 381 Participants, 2019) (Figure 1). In this paper we describe the sedimentology and stratigraphy of the mud-dominated syn-rift sedimentary succession penetrated at IODP Expedition 381 sites M0078 and M0079, positioned in the deep-water, rift axis depocentre within the Gulf of Corinth (Figure 1). We build on previous work on IODP Expedition 381 that focuses on sedimentation rates and general characteristics of the drilled syn-rift succession (McNeill, Shillington, Carter, Everest, et al., 2019). We aim to: (i) characterise the bed-scale sedimentology of mud-dominated basin floor deposits; (ii) use bed-scale variability to identify main stratal packages within the late Quaternary syn-rift depocentre, and (iii) discuss the controls on basin floor sedimentation and stratigraphic evolution in the Corinth Rift. Finally, we discuss the broader implications of our study for understanding controls on syn-rift stratigraphic evolution in rifts, and for interpreting mud-dominated basin-floor deposits in rift settings, including whether or not there are diagnostic criteria to distinguish the range of flow processes and flow triggers in basinal muds.

2 | GEOLOGICAL SETTING

The E-W-trending Gulf of Corinth is the young (<2 Ma), highly active expression of the Corinth Rift that initiated at around 4–5 Ma (Collier & Dart, 1991; Gawthorpe et al., 2018; Hemelsdael et al., 2017, 2021). The basin is 100 km long, up to 30 km wide and over 800 m deep in the main eastern depocentre (Figure 1). The fault-controlled southern basin margin has a narrow shelf (<1 km) and steep slopes (14–18°) compared to more variable shelf widths (up to 12 km) and broad (up to 7 km) gentle slopes (1–2°) along the northern margin (Poulos et al., 1996). The rift cross-cuts the N-S-trending Cretaceous to Oligocene Hellenide fold and thrust belt whose mountainous terrain has been the main clastic sediment source supplying carbonate-rich detritus to the rift (Ford et al., 2013, 2016; Skourtsos & Kranis, 2009). Geodetic and seismicity data document some of the highest extension rates in the world across this rift, with up to 15 mm/yr of N-S extension below the western Gulf, decreasing to 10 mm/yr below the eastern Gulf (e.g. Avallone et al., 2004; Bernard et al., 2006; Briole et al., 2000; Clarke et al., 1998; Davies et al., 1997; Lambotte et al., 2014). Cumulative extensional strain (on geological time scales) is however greatest in the central rift (Bell et al., 2009, 2011; Nixon et al., 2016).

The Corinth Rift evolved in two main phases that are recorded by onshore and offshore deposits (Armijo et al., 1996; Bell et al., 2009; Ford et al., 2007, 2013, 2016; Gawthorpe et al., 2018; Higgs, 1988; Nixon et al., 2016; Sachpazi et al., 2003; Taylor et al., 2011). During Rift Phase 1 (Pliocene, ca. 4 Ma to ca. 2–1.8 Ma; Hemelsdael et al., 2017; Gawthorpe et al., 2018) distributed rifting was confined to the central and eastern northern Peloponnese. Extension was accommodated on normal faults across a broad area and deposition was predominantly continental varying from coarse alluvial deposits in the west, supplied by antecedent river systems, to deep lacustrine deposits in the east (Gawthorpe et al., 2018; Hemelsdael et al., 2017; Rohais et al., 2007). During the transition to Rift Phase 2 (ca. 2–1.8 Ma), fault activity migrated north by ca. 30 km such that the rift depocenter became focused into the Gulf of Corinth, and extension rates increased markedly (Ford et al., 2016; Gawthorpe et al., 2018). Initially both north and south-dipping normal faults controlled Rift Phase 2 depocentres (Bell et al., 2009; Ford et al., 2013, 2016; Nixon et al., 2016). Rift flank uplift and erosion of the southern rift shoulder cannibalised Rift Phase 1 deposits and transverse drainage systems built conglomeratic Gilbert type fan deltas, up to 800 m thick, above north dipping normal faults along the west and central southern basin margin (onshore Middle Group of Backert et al., 2010; Ford et al., 2007, 2016; Gawthorpe et al., 2018; Hemelsdael & Ford, 2016). To the north and east, finer-grained deep-water lacustrine turbidites and basinal mudstones were deposited in the rift axis depocenter (Cullen et al., 2019; Gawthorpe et al., 2018). These deposits are identified as Seismic Unit 1 (SU1 of Nixon et al., 2016; Taylor et al., 2011) on offshore seismic reflection data, and

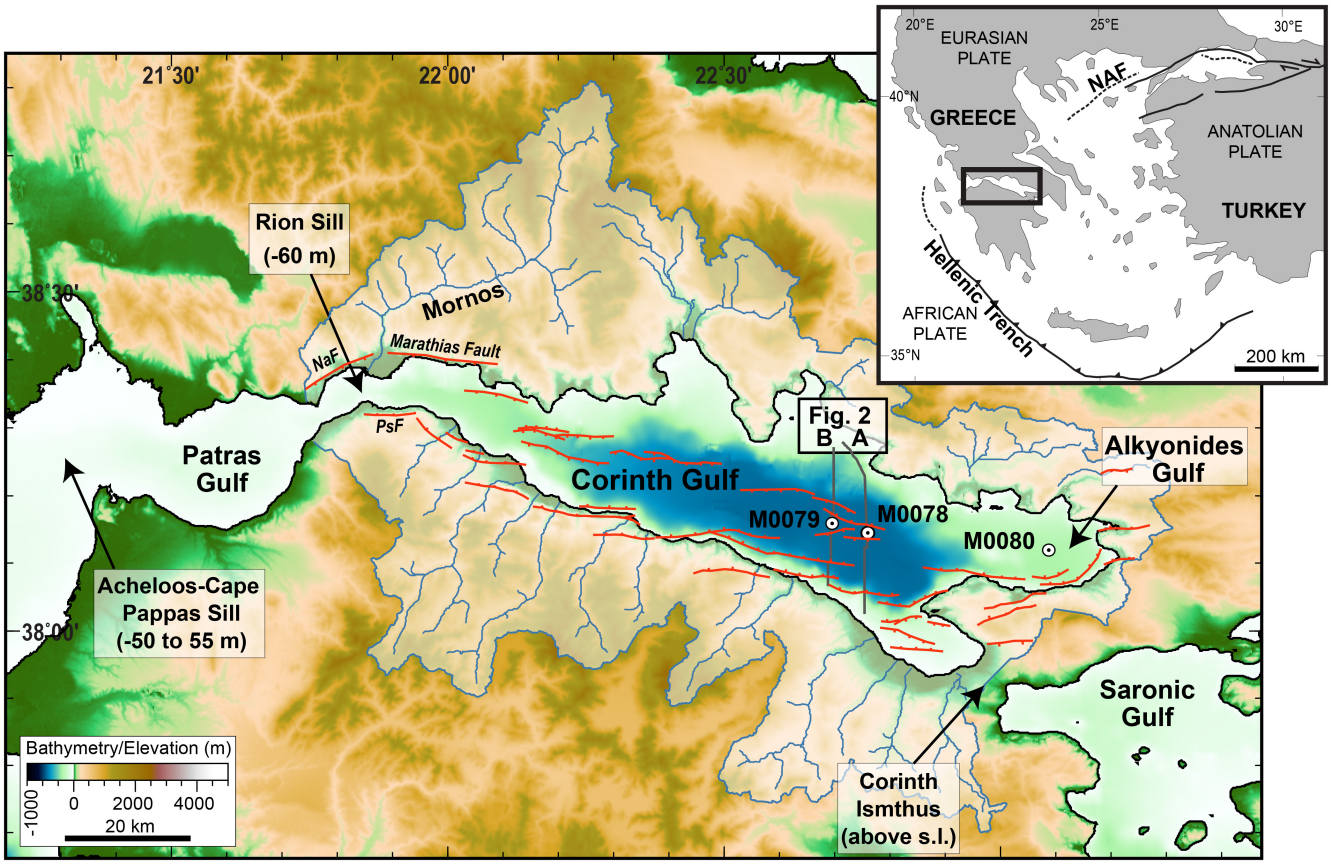

FIGURE 1 Topographic and bathymetric map of the Gulf of Corinth and surrounding area, showing IODP Expedition 381 sites M0078, M0079 and M0080. Main rift faults in red, positions of bounding sills (rift segment boundaries) that controlled ocean access to the Gulf are indicated, as are the main catchment areas and rivers feeding the Gulf (modified from McNeill, Shillington, Carter, Everest, et al., 2019). A and B refer to seismic profiles through sites M0078 and M0079 respectively that are shown in Figure 2. Inset shows regional setting. NaF, Nafpaktos fault; NAF, North Anatolian fault; PsF, Psathopyrgos fault

are characterised by low amplitude reflections that lack continuity (Figures 2 and 3). The upper levels of Seismic Unit 1 were cored in IODP Expedition 381 sites M0078 (385.14–610.43 mbsf) and M0079 (677.23–704.9 mbsf) where it is composed of light grey-to-buff homogenous highly bioturbated muds generally lacking marine microfauna (Lithostratigraphic Unit 2 of McNeill, Shillington, Carter, & Expedition 381 Participants, 2019; Shillington et al., 2019).

A major basin-wide change in seismic facies and locally an unconformity separate Seismic Units 1 and 2. In core this boundary corresponds to an abrupt downhole change from bedded and laminated, greenish-grey mud (Lithostratigraphic Unit 1) to homogenous, light grey-to-buff highly bioturbated muds (Lithostratigraphic Unit 2) (McNeill, Shillington, Carter, & Expedition 381 Participants, 2019; McNeill, Shillington, Carter, Everest, et al., 2019). Between 0.8–0.6 Ma, fault activity again stepped northward in the western and central parts of the rift as strain began to localise on the north-dipping southern border fault of the rift (Figure 1) (Nixon et al., 2016). Fan deltas developed in the hanging walls of newly formed fault segments, and equivalent deposits in the rift axis, imaged on offshore seismic reflection lines comprise alternating high and low amplitude reflection packages (Seismic Unit 2 of Nixon et al., 2016), which have been interpreted as highstand marine and lowstand lacustrine deposits respectively (e.g. Bell et al., 2008, 2009; Lykousis et al., 2007; Sachpazi et al., 2003; Taylor et al., 2011) (Figures 2 and 3). This is supported by marine and lacustrine conditions detected in short cores (Collier et al., 2000; Moretti et al., 2004), and clinoform sequences on some basin margins (e.g. Bell et al., 2008; Leeder et al., 2005; Lykousis et al., 2007; McNeill et al., 2005). These cyclical variations are interpreted to be related to fluctuations in eustatic sea level relative to sill-like boundaries confining the eastern and/or western ends of the rift (e.g. Heezen et al., 1966; Sachpazi et al., 2003). In the west the main sills are the Rion Sill (−60 m) and Acheloos-Cape Pappas Sill (−50–55 m; Figure 1), and in the east, the Corinth Isthmus (emergent at present day) and structural highs within the Saronic Gulf to the east (Figure 1).

Seismic Unit 2 (Figure 2) is correlated with the upper lithostratigraphic package of the succession drilled by IODP Expedition 381 (Lithostratigraphic Unit 1 of Shillington et al. (2019), McNeill, Shillington, Carter, & Expedition 381 Participants (2019), and McNeill, Shillington, Carter, Everest, et al. (2019)), recording the Late Pleistocene and Holocene evolution of the rift (Figure 3). At the sites of the IODP Expedition 381 boreholes, Lithostratigraphic Unit 1 is dominated by mud-rich sediment, with minor sand and silt, and very rare gravels and intraformational slumps. The IODP 381 Science Party recognised two alternating types of subunit within Lithostraigraphic Unit 1: those composed predominantly of homogeneous green-grey bioturbated mud with marine microfauna, and those composed predominantly of laminated and bedded mud of various facies associations, lacking marine microfauna, that were interpreted to reflect isolated/semi-isolated (lacustrine) conditions (McNeill, Shillington, Carter, & Expedition 381 Participants, 2019; McNeill, Shillington, Carter, Everest, et al., 2019; Figure 3). Deposition in both types of sub-unit was interpreted to have been mainly from suspension settling and dilute turbidites in a deep-water, rift axis location (McNeill, Shillington, Carter, & Expedition 381 Participants, 2019; McNeill, Shillington, Carter, Everest, et al., 2019).

3 | DATA AND METHODOLOGY

In this study we use cores from the IODP Expedition 381: Corinth Active Rift Development (McNeill, Shillington, Carter, & Expedition 381 Participants, 2019; McNeill, Shillington, Carter, Everest, et al., 2019). The expedition was conducted in the eastern Gulf (Figure 1) from the 23rd of October to the 18th of December 2017, with the Onshore Science Party (OSP) held at the IODP Bremen core repository from the 31st of January to the 28th of February 2018. This study focuses on sites M0078 and M0079 located in the rift axis in water depths of ca −860 m, and particularly on the sedimentology and stratigraphy of Lithostratigraphic Unit 1 (Figure 3), which represents the uppermost 385 m at Site M0078 and 680 m at Site M0079. The boreholes were continuously cored with core recovery of >87% (McNeill, Shillington, Carter, & Expedition 381 Participants, 2019; Shillington et al., 2019).

Building upon visual core descriptions of the OSP and other data collected during the OSP, such as palaeomagnetic, micropalaeontological, geochemical and physical property data (McNeill, Shillington, Carter, & Expedition 381 Participants, 2019; McNeill, Shillington, Carter, Everest, et al., 2019), we performed high-resolution bed-scale logging (down to millimetre scale) on the first 307 m of sediments at Site M0079 (Subunits 1–1 to 1–5 of McNeill, Shillington, Carter, & Expedition 381 Participants, 2019; McNeill, Shillington, Carter, Everest, et al., 2019; Figure 3). This site was selected because of its expanded sedimentary succession that enables more detailed analysis of the basin floor sedimentology. More than 12,000 beds, defined by abrupt changes in colour and grain size, are recognised within the upper 307 m of M0079. Detailed core sedimentological description was supplemented by grain size analysis, and optical and scanning electron microscopy of selected samples. This systematic analysis of beds has been applied to the whole of Lithostratigraphic Unit 1 in boreholes M0079 and M0078, providing new insight into the full sedimentological and stratigraphic characteristics of Lithostratigraphic Unit 1 and the evolution of the rift over the last ca. 800 ka.

Grain size analysis was performed on 12 U-channels and a range of spatula samples at a sampling spacing of respectively 3–5 mm and 1–2 cm using a Mastersizer 3000 from Malvern Panalytical. Samples were analysed 5 times for reproducibility and the average values for each grain-size fraction were used to provide a D_{50} value of the grain-size distribution. A total of twenty samples from the range of bed-types were selected for polished thin sections oriented normal to bedding. Thin sections were scanned using an Epson V700 photo scanner at 2400 ppt resolution and microscopic descriptions were performed using an optical Nikon Eclipse LV100N polarised microscope. A ZEISS Supra 55VP scanning electron microscope fitted with a HDAsB backscatter detector was used for observations at 15.00 kV, with an aperture of 60 µm and working distance of ca. 9 mm. Qualitative elemental analyses were performed to recognise the mineral composition of samples.

Six samples of aragonite laminations from Site M0079 were selected for dating using Th/U isotope analysis (Table S1; Supplementary Material). In order to reduce calcite contamination in these samples, we used the magnetic separation method of Hang et al. (2014). During this procedure aragonite is coated by a cobalt magnetic stain and therefore, can be magnetically separated from calcite, which remains unstained. Following separation, all samples were processed for Th/U isotope analysis on a Nu Plasma II™ MC-ICP-MS (see details in Supplementary Materials).

4 | BED-SCALE SEDIMENTOLOGY

Lithostratigraphic Unit 1 (McNeill, Shillington, Carter, & Expedition 381 Participants, 2019; McNeill, Shillington, Carter, Everest, et al., 2019; Figure 3) is dominated by unlithified carbonate-rich muds, having more than 50% clay-grade and silt-grade particles of grain sizes less than

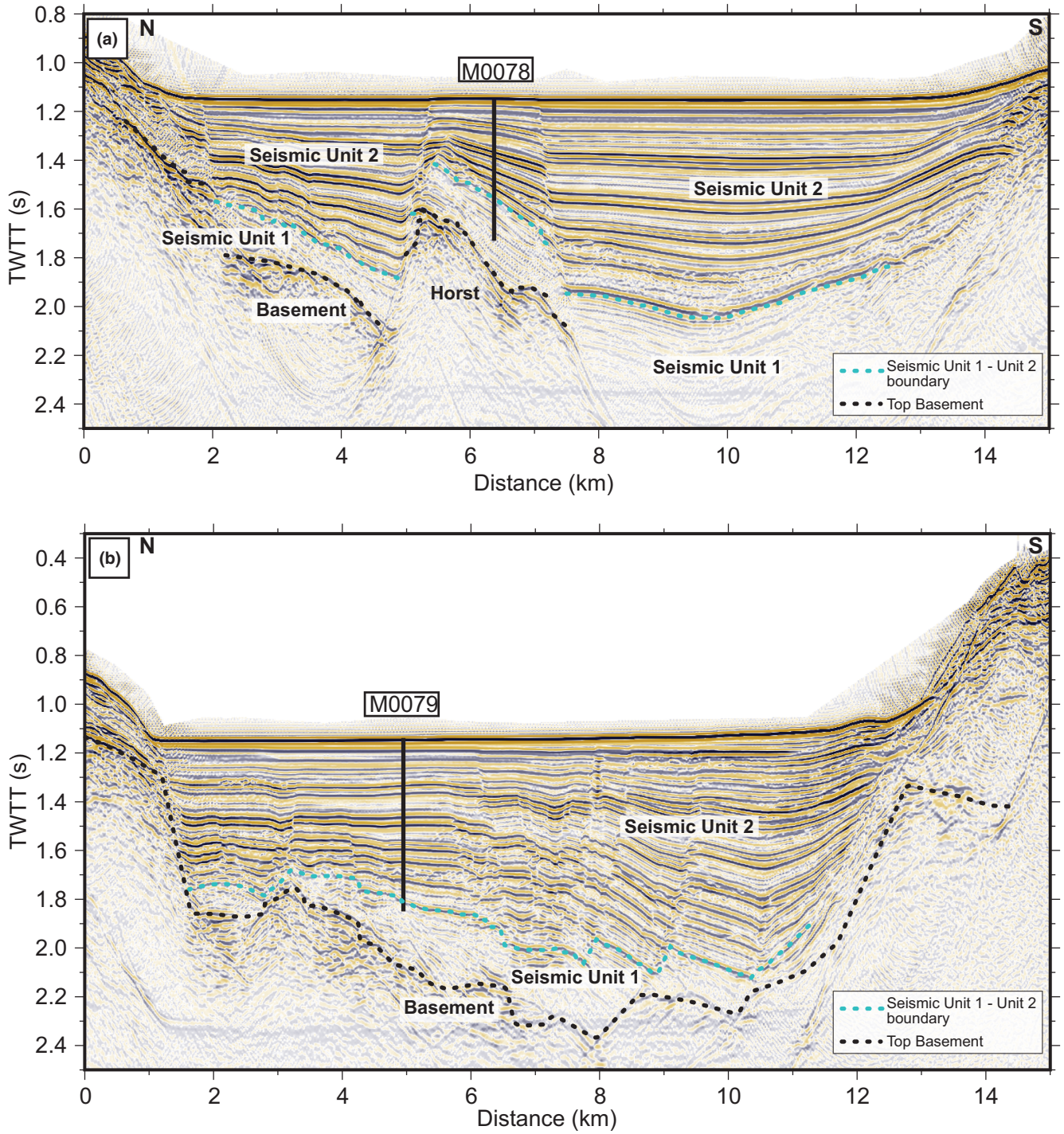

FIGURE 2 Dip section seismic lines crossing through the IODP 381 sites M0078 and M0079. (a) R/V Maurice Ewing line 42, across site M0078, and (b) R/V Maurice Ewing line 41, across site M0079. The black dashed line depicts the top of pre-rift basement and the light blue dashed line depicts the boundary between Seismic Unit 1 and Seismic Unit 2 of Nixon et al. (2016) which are equivalent to IODP Expedition 381 Lithostratigraphic Unit 2 and Lithostratigraphic Unit 1 respectively (McNeill, Shillington, Carter, & Expedition 381 Participants, 2019; Shillington et al., 2019)

62.5 μm (Lazar et al., 2015). Grain size is predominantly fine silt grade, but with occurrence of some very fine and fine sand and rare coarser-grained graded beds. Detrital calcite predominates with subordinate quartz, feldspar, and phyllosilicates, indicating the basin fill is dominated by clastics derived from the rift margin catchments. Colour variations mirror subtle compositional and grain size changes with darker hues typical of coarser grain sizes. Greenish grey and medium to dark grey hues predominate. We have identified a number of distinctive bed types

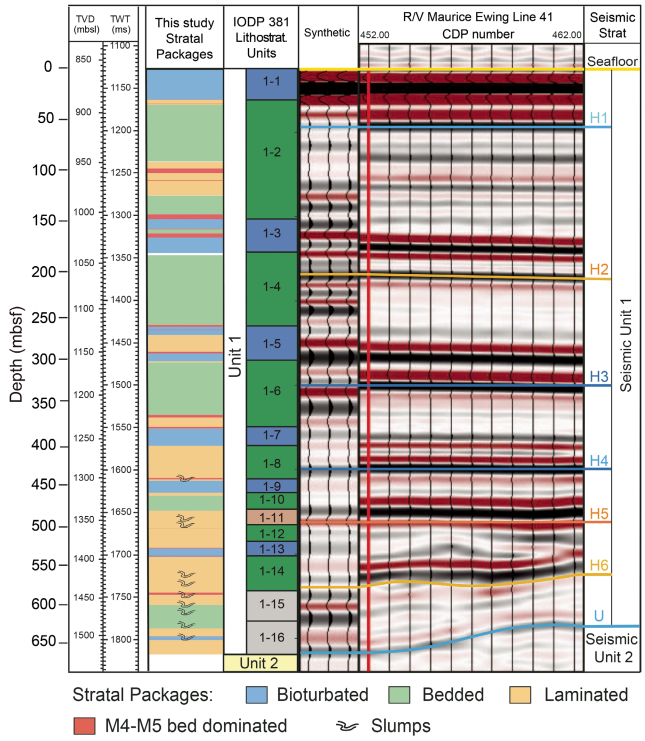

FIGURE 3 Existing seismic stratigraphy and IODP Expedition 381 lithostratigraphy of the Gulf of Corinth compared to the stratal packages defined in this paper using site M0079 as an example. Seismic stratigraphy after Nixon et al. (2016); IODP Expedition 381 lithostratigraphic units and sub-units after McNeill, Shillington, Carter, and Expedition 381 Participants (2019) and Shillington et al. (2019)

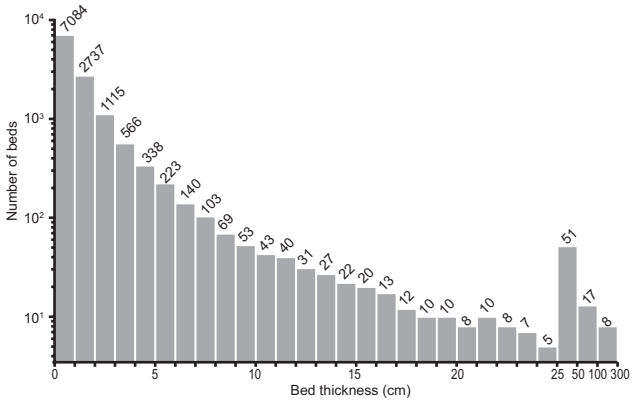

FIGURE 4 Histogram showing frequency of bed thicknesses (in cm) within the first 307 m at site M0079. Note scale change on bed thickness axis at 25 cm

within Unit 1, based on core observation of bed contacts, colour, grain size and grain size trends, and sedimentary and biogenic structures, which have been supplemented by grain size analysis, and optical and electron-optical petrography. A bed (a genetic bed, sensu Campbell, 1967) is defined between two sharp boundaries marked by changes in one or more of grain size, colour, sediment texture or intensity of bioturbation. Based on these parameters, the vast majority, ca. 80% of beds are <2 cm thick (Figure 4) and can be divided into four major bed type groups: (i) homogeneous and laminated mud beds, (ii) highly bioturbated beds, (iii) graded beds, and (iv) matrix-supported conglomerates and slumped beds (Figure 5). In the following sections we describe the bed types within each of these groups and interpret the processes responsible for their deposition.

4.1 | Homogeneous and laminated mud beds

These mud beds are typically <2 cm thick, have sharp planar bed boundaries, commonly present no internal grain-size change discernible to the naked eye, and appear to be homogeneous, lacking sedimentary structures, or they may contain millimetre to sub-millimetre lamination, continuous at the scale of the core. Variations in these characteristics define five mud bed types; homogenous mud beds (M1), and four types of laminated mud beds (M2 to M5) (Figure 5). The mud beds are distinguished from graded beds by not showing an abrupt visible increase in grain size at their base compared to the underlying bed, and/or not showing an upward-fining trend within a bed.

4.1.1 | Homogeneous mud beds (M1)

These greenish grey calcareous mud beds are generally homogeneous in core, up to a few centimetres thick, and have relatively sharp, planar, continuous bed boundaries at core scale (Figure 6a,g). Colours vary from light greenish grey (GLEY 1 7/10Y on the Munsell soil colour scale) to grey (GLEY 1 5/N) to dark grey (GLEY 1 4/2). Rare reddish-brown hues also occur (5YR 6/2 to 7.5YR 5/2). Colour tones are generally homogeneous, but may lighten or darken upward subtly. The beds are usually structureless, but may be subtly laminated. Homogeneous mud beds are generally unbioturbated, but in rare cases the top of beds may be weakly bioturbated (Bioturbation Index [BI] = 1 to 2), predominantly by simple millimetre-diameter, non-lined burrows sub-parallel to bedding (*Planolites*), or by unidentified diffuse burrows picked out by slight colour mottling (Figure 6a, inset detail).

Interpretation: The absence of macrofauna and the paucity of bioturbation indicate a non-marine or stressed depositional environment. Homogeneous muds may be deposited (i) out of suspension from the water column as hemipelagites (Ochoa et al., 2013), or (ii) by deposition

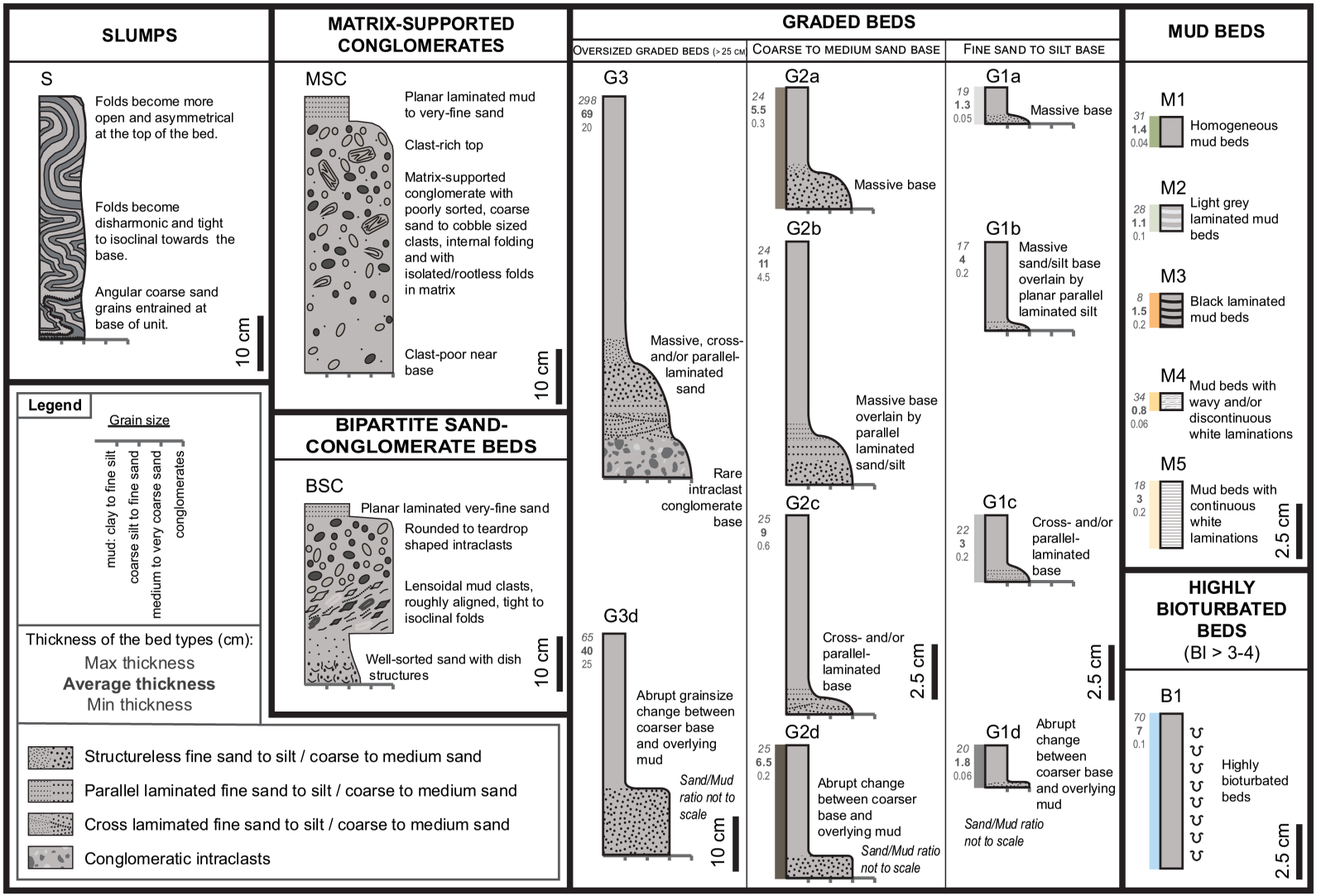

FIGURE 5 Bed type classification for Lithostratigraphic Unit 1. Graphic logs of each bed type include grain size and thickness variations. Four major bed type groups are identified: Homogeneous and laminated mud beds (M1–M5); highly bioturbated beds (B1); graded beds (G1–G3); and matrix-supported conglomerates and slumped beds (slumps (S), matrix-supported conglomerates (MSC) and bipartite sand-conglomerate beds (BSC)), colour codes for bed type and abbreviations are used in other figures

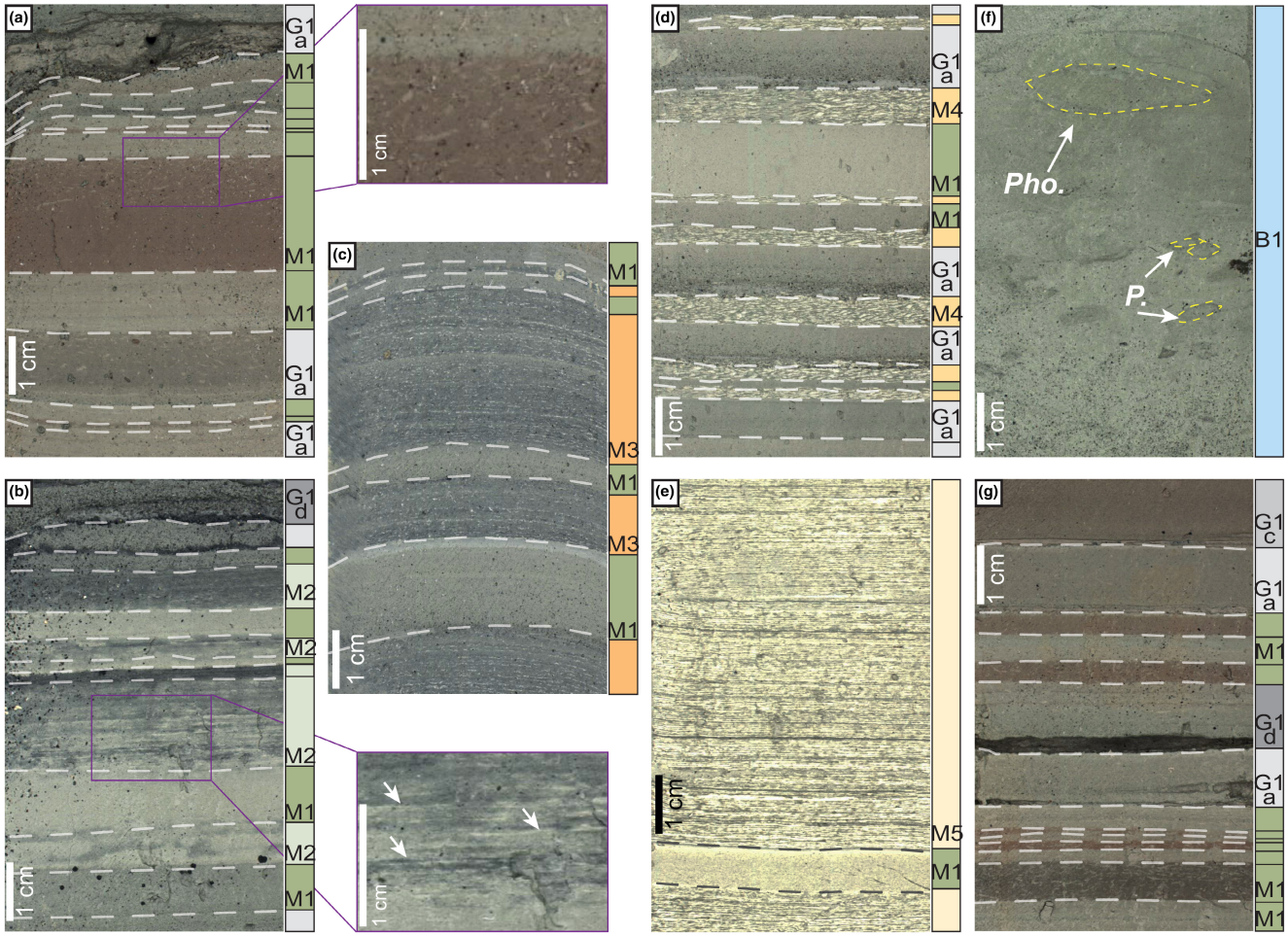

FIGURE 6 Core photographs from site M0079 showing examples of mud beds and highly bioturbated beds. (a) M1 homogeneous muds with G1a graded beds (inset: Detail of bioturbated top of M1 mud bed). (Core 54R-3, core depth 116–124 cm, borehole depth 206.46–206.54 mbsf). (b) M2 light grey laminated mud beds; inset detail shows wavy tops of M2 laminations (highlighted at arrowheads) (Core 65R-3, core depth 22–30 cm, borehole depth 257.52–257.6 mbsf). (c) Interbedded M3 black laminated muds with M1 homogeneous muds (Core 31V-4, core depth 19–30 cm, borehole depth 121.66–121.77 mbsf). (d) M4 discontinuous white laminated muds (with discontinuous laminations) interbedded with G1a graded beds (Core 73R-2, core depth 39.5–47 cm, borehole depth 296.195–296.27 mbsf). (e) M5 mud beds with continuous white laminations (Core 45R-2, core depth 5–13 cm, borehole depth 166.82–166.93 mbsf). (f) B1 highly bioturbated muds; Pho. (*Phoebichnus*) and P. (*Planolites*) ichnotaxa highlighted (Core 68R-2, core depth 78–86 cm, borehole depth 271.58–271.69 mbsf). (g) Interbedded M1 homogenous muds with G1a, G1c and G1d graded beds; note the bioturbated top to the G1c upper mud layer (Core 55R-2, core depth 98.5–106.5 cm, borehole depth 209.785–209.865 mbsf)

out of waning low-density turbidity currents (sensu Lowe, 1982), or (iii) by the deceleration of quasi-laminar or laminar, low strength and low velocity plug flows, as the most distal products of density underflows that may have been lower density turbidity currents up-dip (Baas et al., 2011). Occurrence of subtle lamination would imply a component of tractional reworking during suspension fallout, confirming deposition from a waning, low-density turbulent flow. Variations in mud colour are interpreted to represent variation in organic content and degree of oxidation of this disseminated organic matter, and possibly minor variations in sediment composition. M1 beds without bioturbation imply dysoxic conditions on the basin floor. Bioturbated bed tops suggest that one or more oxygenated underflows have passed over the bed and at least temporarily allowed colonisation of the uppermost sediment by polychaetes or other soft-bodied fauna. In the case of an M1 bed with a bioturbated top having been deposited by freezing of a plug flow, the density underflow itself or a dilute, oxygenated tail to the same flow may have sufficiently oxygenated the uppermost sediment of the bed to allow temporary colonisation.

4.1.2 | Light grey laminated mud beds (M2)

These centimetre-thick calcareous mud beds are typically characterised by weakly developed millimetre to

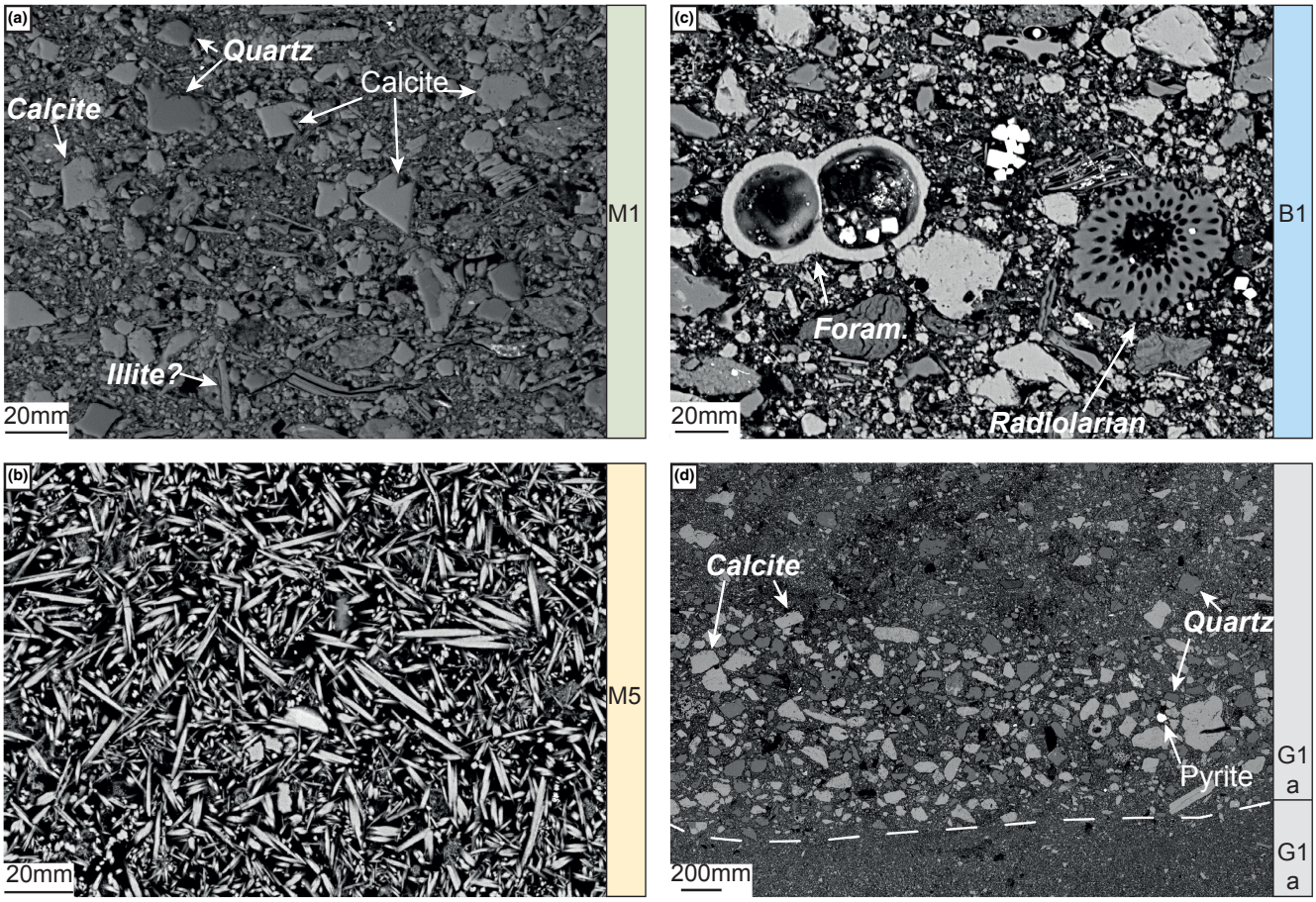

FIGURE 7 (a) BSEM image of M1 homogeneous mud (Core 54R-3, core depth 118–122 cm, borehole depth 206.48–206.52 mbsf). (b) SEM image, aragonite needles making up M5 mud beds with continuous white laminations (Core 45R-2, core depth 8–10 cm, borehole depth 166.89–166.91 mbsf). (c) SEM image, highly bioturbated and poorly sorted B1 muds, with foraminifera, radiolarian and bubbled volcanic glass shard (top centre of field of view) (Core 75R-1, core depth 136–140 cm, borehole depth 305.66–305.70 mbsf). (d) SEM image, sharp-based and fining-up fine sand basal layer of G1a graded bed (Core 71R-1, core depth 112–116 cm, borehole depth 285.42–285.46 mbsf). All samples from site M0079

sub-millimetre thick parallel laminations (Figure 6b). Sorting is moderate to poor, with mainly detrital carbonate grains (Figure 7a). The lamination is defined by subtle colour variations, with colours varying from light greenish grey to light grey (GLEY 1 5/10Y to 6/10Y and 6/5GY). Many laminations are laterally continuous at the core scale, whilst others infill millimetre-scale erosional scours, or may be discontinuous, or undulatory with millimetre amplitude and centimetre-scale wavelength (Figure 6b, inset detail). Occasionally, the lower part of a bed is lighter in colour than the upper part. Bioturbation is typically absent, although the uppermost part of beds may be very weakly bioturbated (BI = 1), by simple, millimetre-diameter burrows of *Planolites*.

Interpretation: Subtle erosional contacts suggest bypass and scouring by low energy turbidity currents. The infill of shallow scours by parallel-bedded and wavy to discontinuous laminations, and the subtle normal grading implied by darkening-up colour changes are indicative of deposition out of waning, low-density turbidity currents with a component of tractional reworking (Talling et al., 2012). The colour grading may reflect compositional changes as well as grain size changes, with an upward increase in organic content and possibly phyllosilicates within individual laminations. The millimetric scale of laminations suggests deposition out of very low-energy, though still turbulent, dilute underflows and with a lower sedimentation rate compared to the centimetre-scale bedding of M1 homogeneous muds. Restriction of bioturbation to a few bed tops and the absence of macrofauna implies a stressed environment, possibly resulting from abnormal salinity or dysoxic conditions.

4.1.3 | Black laminated mud beds (M3)

These, typically 1–2 cm thick, laminated mud beds (Figure 6c) consist of millimetre to sub-millimetre thick

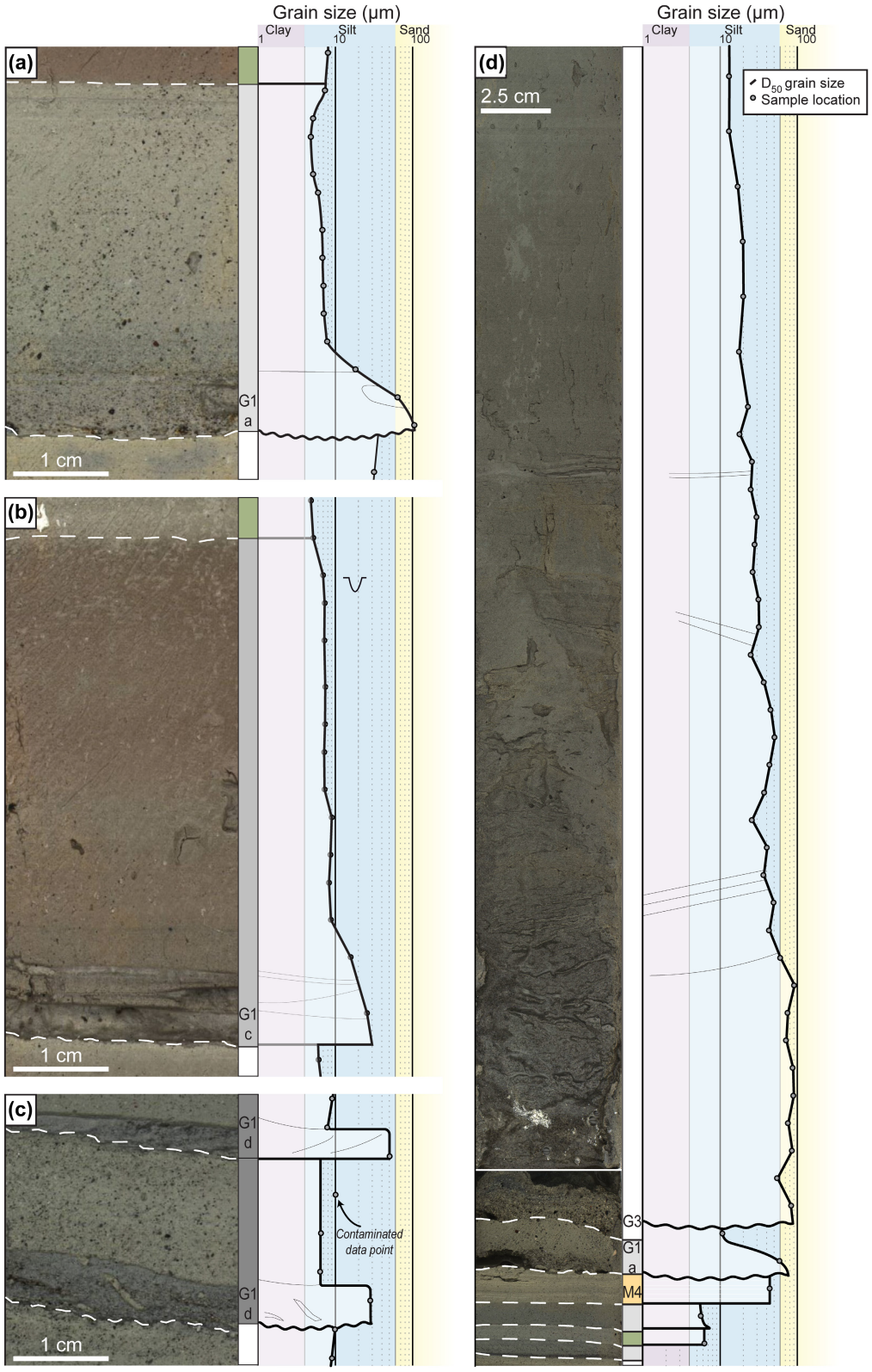

FIGURE 8 Core photographs from site M0079 showing examples of graded beds. Log sections and grain size analyses (D_{50} value of the grain-size distribution) are shown next to each core photograph. (a) G1a bed (Core 55R-3, core depth 59.5–63.5 cm, borehole depth 210.895–210.935 mbsf). (b) G1c bed (Core 55R-2, core depth 107.5–112.5 cm, borehole depth 209.875–209.925 mbsf). (c) G1d bed (Core 75R-2, core depth 128.5–131 cm, borehole depth 307.085–307.11 mbsf). (d) G3 bed (Core 71R-3, core depth 110–150 cm and Core 71R-4, core depth 0–5 cm, borehole depth 288.4–288.85 mbsf)

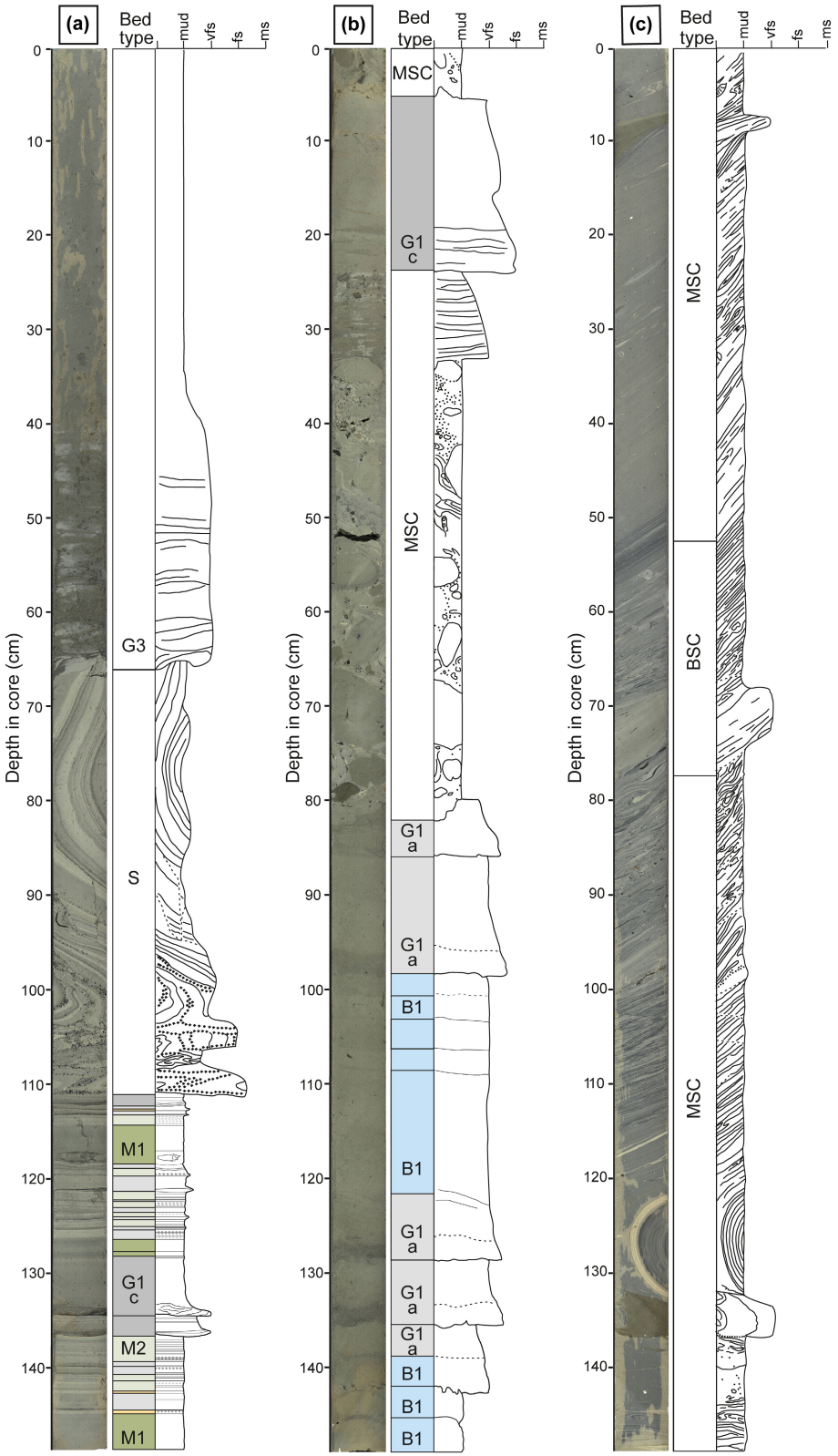

FIGURE 9 Core photographs from site M0079 showing examples of (a) example of a slumped bed occurring above interbedded homogeneous (M1) and laminated (M2) mud beds and G1 graded beds and overlain by an oversized graded bed (G3) (Core 85R-3, core depth 0–150 cm, borehole depth 356.00–357.50 mbsf), (b) matrix-supported conglomerate (MSC) overlying highly bioturbated (B1) and graded beds (G1a). Also note the overlying graded bed (G1c) (Core 107R-1, core depth 0–150 cm, borehole depth 458.40–459.90 mbsf), and (c) matrix-supported conglomerates (MSC) and a bipartite sand-conglomerate bed (BSC) (Core 113R-3, core depth 0–150 cm, borehole depth 490.40–491.90 mbsf). Colour codes refer to bed types in Figure 5

laminations alternating between black to dark grey (GLEY 1 4/N to 3/N) mud and grey mud (GLEY 1 6/N-5/N). The laminae of the two colours may be of equal thickness or paler laminations may be thinner, and occasionally wavy and more discontinuous than the darker laminae. All laminations are laterally continuous at the core scale. Bioturbation is absent or rarely developed on bed tops (as in M2).

Interpretation: The darker grey to black colours of M3 imply higher concentrations of dispersed organic matter than present in M2 light grey laminated mud beds. Internally, homogeneous laminae may be the product of suspension fall-out from the water column as hemipelagites (Ochoa et al., 2013), with varve-like fluctuations between the lighter and darker laminae indicating short-term (possibly annual or seasonal) changes in sediment input, bottom-water oxygenation and rates of settling of organic-rich hemipelagite. Alternatively, the lamination may record tractional processes within thin, fine-grained deposits of waning, low-density turbidity currents (Lowe, 1982). The lack of macrofauna and alternations of zero to low levels of bioturbation indicate a stressed, potentially non-marine environment (Gingras et al., 2011).

4.1.4 | Mud beds with wavy and/or discontinuous white laminations (M4)

These laminated mud beds are typically 0.5 cm to a few centimetres thick and characterised by thin, millimetre to sub-millimetre laminations alternating between light greenish grey (GLEY 8/10Y) to light grey or white (GLEY 7/N to 8/N), and grey to greenish grey (GLEY 6/N to 6/10Y) mud. The lighter laminae are generally discontinuous, faint or disrupted (Figure 6d). The base of M4 beds is sharp but non-erosive, and the tops of beds may contain inclined, discontinuous laminations and/or have an irregular or erosional contact when beneath graded beds. Compositionally, white laminations may be aragonite-rich or calcite-rich. Where aragonite-rich, a characteristic needle-like morphology is well developed, as in M5 muds. Aragonite needles are up to 25 μm in length and stellate clusters of needles are also observed. The grey to greenish grey laminations comprise mainly clay and silt-sized detrital carbonate grains. The M4 beds are usually non-bioturbated, but when underneath highly bioturbated mud beds (B1) they can exhibit a low diversity, low abundance (BI = 1 to 2) ichnofauna.

Interpretation: The wavy to discontinuous white laminations within M4 mud beds denote hemipelagic sedimentation. Palaeoenvironmental conditions are inferred to have fluctuated between, (i) periods that promoted high precipitation of aragonite or calcite in the water column (e.g. aragonite whitings), most-likely during summer seasons with elevated temperatures and possible algal blooms that would have extracted CO2 from the Gulf's waters (e.g. Richter et al., 1993; Sondi & Juracic, 2010), and (ii) cooler, wetter winter seasons, with greater detrital and organic input and without aragonite whitings (Razum et al., 2021). Thus, we interpret M4 laminations to represent seasonally varved hemipelagites. The discontinuous or wavy nature of some M4 white laminations suggests that whitings were weak in some seasons. The inclined fabric and eroded tops that are overlain by graded (turbidite) beds may record shear of unconsolidated laminations on the basin floor by overriding turbidity currents.

4.1.5 | Mud beds with continuous white laminations (M5)

These distinctive centimetre- to decimetre-thick laminated mud beds are characterised by pin-striped, parallel laminations marked in core by millimetre to sub-millimetre alternations of white/light grey (GLEY 1 8/N to 7/N) and darker grey to greenish grey (GLEY 6/N to 6/10Y) mud laminations (Figure 6e). Occasional thicker, isolated light laminations of up to 1–2 mm are observed. Typically, ca. 20 alternations of colour occur per centimetre. Laminations can be traced over the width of the core, although with some variation in prominence of the whitish laminations. The light-coloured laminations are composed predominantly of either calcite or aragonite, but commonly the whitish laminations contain well-sorted, silt-sized, elongate aragonite needles with some stellate clusters. Aragonite is the dominant constituent (>90%) in the thicker, whitish laminations (Figure 7b). The darker laminations comprise well-sorted, sub-rounded to sub-angular, fine silt to clay-sized grains of calcite, together with diatoms, quartz and pyritized organic-rich grains. Bioturbation is mainly absent, but beneath highly bioturbated mud beds (B1) bioturbation may be moderate (BI = 2 to 3), consisting of a low-diversity ichnofauna of *Teichichnus* and *Planolites*.

Interpretation: The alternating white and darker laminations are interpreted to indicate varved, seasonal hemipelagic sedimentation. Aragonite precipitation is interpreted to have occurred during hot summer months, as interpreted for M4 beds, (Razum et al., 2021; Richter et al., 1993). The presence of rare decimetre-scale thicknesses of M5 mud beds imply that there were periods of hundreds of years, based on a representative 1 cm per 20 years deposition rate from typical annual varve thicknesses, with no visible record of turbidity currents reaching Site M0079 on the distal basin floor.

4.2 | Highly bioturbated beds (B1)

Highly bioturbated beds have a distinctive greenish grey (GLEY 1 6/10Y to 5/5GY) colour and are poorly stratified although indistinct laminations and beds can be distinguished by subtle changes in colour, bioturbation type and intensity, or grain size (Figure 6f). Beds are typically several centimetres thick, but can be up to several tens of centimetres. Where beds are discernible, they commonly have sharp bases and sharp to gradational tops. Some graded beds (see Section 4.3) with sandy bases can be identified and these commonly fine upward from fine or medium sand into highly bioturbated muds. Remnant sedimentary structures in these coarser beds include parallel and cross-lamination, suggesting they are bioturbated equivalents of silty and sand-based G1, G2 and G3 graded beds (see Section 4.3). Bioturbation intensity is generally high (BI > 4) and often complete (BI = 6). At high intensities, burrow-mottled intervals show no record of pre-existing sedimentary structure and reveal few discernible ichnotaxa. Where bioturbation is of slightly lower intensity, identifiable ichnotaxa include *Thalassinoides*, *Planolites*, *Teichichnus*, *Palaeophycus*, *Helminthopsis*, *Phycosiphon* and *Chondrites*. As well as the diversity of bioturbation, another distinctive feature of this bed type is that they are fossiliferous. Bioclasts include fragments of gastropods and bivalves, and microfossils including benthic and planktonic foraminifera, calcareous nannofossils and diatoms (Figure 7c). Clastic grains are dominated by carbonates, with subordinate quartz, feldspar, and phyllosilicates. Sorting is poor. Dark flecks of pyritized organic matter also occur scattered within B1 mud beds.

Interpretation: Where bioturbation is complete it is not possible to determine whether the muds originally included parallel laminations or other sedimentary structures that might have indicated a turbiditic origin as opposed to a homogeneous mud of hemipelagic or quasi-laminar flow origin (Baas et al., 2011; Lowe, 1982; Ochoa et al., 2013). However, remnant parallel laminations and grain size fluctuations are interpreted as a window into tractional structures which would imply that a significant proportion of the highly bioturbated beds were deposited by low-density turbidity currents. The macro- and microfauna present within the highly bioturbated beds indicate a marine environment. The presence of benthic foraminifera and the diverse range and pervasive high intensities of bioturbation indicate that the basin floor was well oxygenated during deposition.

4.3 | Graded beds

This group of beds is characterised by their sharp, planar to erosive bases, and step increase in grain size compared to the immediately underlying bed. They show a demonstrable fining-up from a lower coarser-sized interval to an upper mud-grade interval. They are subdivided based on the grain size and sedimentary structures of the coarser lower portion of the bed, the nature of grain size variations, and bed thickness (Figure 5). Graded beds are the most frequent bed types in the studied succession.

4.3.1 | Graded beds with silt to fine sand bases (G1)

These sharp, planar to slightly erosive based beds, typically a few centimetres thick, have a thin basal layer of silt to very fine sand, ranging in thickness from a few grains up to 5 mm thick (Figure 5). Beds are laterally continuous on the core scale. We subdivide G1 beds on the basis of the internal character of the basal layer into those that are massive and structureless (G1a, Figure 8a), those with a massive sand base, overlain by parallel-laminated silts (G1b), and those with cross- or parallel lamination (G1c, Figure 8b). A further variation is recognised, in which the transition from the coarser-grained basal layer to the overlying mud layer is abrupt (G1d) (Figure 8c). Additional examples are illustrated in Figure 6a,b,d,g. The basal coarser portion of the beds is generally darker in colour (GLEY 1 6/N) than the overlying mud interval and may contain charcoal or wood fragments and pyrite. The upper mud interval of G1 beds is similar to homogeneous mud beds (M1) and in rare cases contain weak laminations, or show sparsely bioturbated tops (e.g. the G1c bed in Figure 8b). Microscopy reveals the very fine to fine sands of the basal layer to be poorly sorted and to have sub-angular to sub-rounded grain shapes (Figure 7d). Compositionally, grains are dominated by detrital carbonate, with subordinate quartz and feldspar, and minor phyllosilicates, reworked bioclasts and rare volcanic glass shards.

Interpretation: The features of sharp or erosional base, normal grading, and tractional sedimentary structures in the basal layer together indicate that G1 graded beds are the deposits of waning, low-density turbulent underflows (Lowe, 1982; Mulder & Alexander, 2001). Where weak laminations persist or reappear in the upper mud layer, this is interpreted to indicate that tractional reworking continued during deposition from the dilute tail of the turbidity current. Where the muds are massive, deposition may have been from the dilute tail of a turbidity current, or from freezing of a terminal low-velocity and low-strength quasi-laminar or laminar plug flow (Baas et al., 2011). G1 graded beds may occur as isolated beds within otherwise highly bioturbated mud (B1), in which case a marine depositional environment is inferred. In the absence of an

associated varied marine fauna and microfauna and reworking of sedimentary structure by intense bioturbation, particularly in the upper mud layer, G1 graded beds are interpreted as non-marine deposits. Where a bed-top shows low intensity bioturbation (BI = 1 to 2), the implication is that the causal turbidity current or subsequent bypassing turbidity currents carried oxygenated waters down onto the distal basin floor, allowing temporary colonisation of the basin floor sediment by a limited infauna.

4.3.2 | Graded beds with medium to very coarse sand bases (G2)

These sharp planar to erosive based beds have a distinctive basal grey to dark grey (typically GLEY 1 6/N), medium to very coarse sand interval that grades upward into mud (G2a, b, c, Figure 5). Alternatively, the basal coarser layer may have a relatively abrupt contact with the overlying mud-dominated part of the bed (G2d). Compared to the silt to fine sand-based beds, these medium to very coarse sand-based beds are generally thicker, being several centimetres to a few tens of centimetres thick. The basal coarse interval is either structureless, planar and/or cross-laminated, or shows an upward transition from a structureless base to parallel lamination. Plant and shell fragments, granule to small pebble sized intraclasts, and limestone pebbles may be present. The upper mud interval is similar to the homogeneous mud beds (M1) with rare weak lamination and little or no bioturbation. Scattered plant debris may occur within the mud interval.

Interpretation: G2 graded beds show the same range of sedimentary structures, textures and compositional characteristics as G1 graded beds. They are therefore similarly interpreted as the deposits of waning, low-density turbidity currents and detailed interpretations of flow types for each component of the graded beds are similar to those for the G1 graded beds. The coarser basal grain sizes and greater bed thicknesses denote, however, deposition out of more energetic and/or more prolonged flows.

4.3.3 | Oversized graded beds (G3)

These major graded beds range in thickness from 25 cm to ca. 2 m and are characterised by an erosive base, overlain by a centimetre- to decimetre-thick layer of coarse to medium sand, rarely conglomerate (medium pebbles), that grades gradually (G3, Figure 8d) or abruptly (G3d) up through finer sand to silt and mud. The sandy base is either massive or includes parallel- or cross-laminations when a gradual transition is visible. Where massive, dish structures are common. Mud clasts are rare, but may be found close to the base of the bed. An abrupt grain-size transition to the overlying mud interval in G3d beds, producing a sand-mud couplet, and is usually associated with a structureless basal sand interval. Sands are dark grey with pyrite and organic material commonly present (GLEY 1/6 N). Mud and fine silt intervals typically represent 50%–80% of total bed thickness and are generally homogeneous, but can show rare weak lamination. Colour tones can lighten in steps or gradually, up through the mud layer.

Interpretation: These beds are interpreted to represent initial rapid deposition of sediments, as indicated by the massive structureless sand, associated with 'high-density', turbulence-supressed turbidity currents (sensu Lowe, 1982; Talling et al., 2012). The dish structures imply rapid dewatering immediately after deposition. Normal grading and parallel lamination of the upper basal layer signify rapid deceleration of the flow and a reduction of sediment concentration within the overriding flow, transitioning to a low-density turbidity current. The planar laminations are characteristically produced by tractional reworking by a more dilute flow (Allen, 1982; Best & Bridge, 1992). As with G1 and G2 beds, where weak laminations are apparent in the upper mud layer, this implies continued tractional reworking during deposition out of suspension of the waning, low-density turbidity current. Where the muds are homogeneous, deposition may again be out of suspension from the dilute tail of the underflow (sediment lost from the flow) or by rapid deceleration of a quasi-laminar or laminar plug flow (after sediment entrainment into the flow).

4.4 | Matrix-supported conglomerates and slumped beds

Matrix-supported conglomerates displaying varying degrees of ductile and brittle deformation have been observed at several intervals within the cores. Two end-member types of matrix-supported conglomerates are recognised that commonly occur together (Figure 5). In addition, slumped intervals, occur in association with, and also unrelated to, matrix-supported conglomerates.

4.4.1 | Slumps (S)

Slumps occur as isolated beds up to 20–50 cm thick of coherent, highly contorted (folded and faulted) intraformational usually laminated sediments (Figure 9a). The sediments that have undergone ductile deformation have a slightly higher silt and fine sand content when compared with more thinly laminated muds that have reacted

in a more brittle fashion to displacement. In thicker folded units, folds tend to be disharmonic and tight to isoclinal towards the unit's base, transitioning through moderately inclined to recumbent folds, to more open, asymmetrical folds towards the unit top. Black angular grains of coarse sand to fine gravel size can often be observed in the lower portion of the deposit, entrained between detached folds and within rare fault zones. The basal contact with the underlying autochthonous sediments is sharp. Slumped units are frequently overlain by sandy graded beds, as is the case with the matrix-supported conglomerates, suggesting an association between these depositional processes.

Interpretation: The deformation features in this bed type are generated by shear folding and faulting characteristic of slump deposits (e.g. Alsop & Marco, 2013; Gawthorpe & Clemmey, 1985; Martinsen & Bakken, 1990; Moore, 1961). The relatively thick laminations, coupled with a higher silt and fine sand content, may have resulted in a higher intergranular porewater content that facilitated a plastic style of deformation when slope failure occurred. The basal disharmonic and tight to isoclinal folds may represent drag folds associated with high shear transport and emplacement (e.g. Martinsen & Bakken, 1990). Angular coarse sand to fine gravel clasts appear to have been entrained through the base of the deposit, signifying a degree of friction or coupling with the underlying substrate (i.e. no evidence for hydroplaning), as also indicated by basal drag folds.

4.4.2 | Matrix-supported conglomerates (MSC)

The first distinctive type of matrix-supported intra-clast conglomerates are up to 2 m thick, containing poorly-sorted subangular to subrounded clasts, ranging in size from granules to cobbles within a grey mud matrix (Figure 9b,c). Clasts, are typically composed of mm-scale laminated muds that are commonly internally folded and may also exhibit extensional faulting. Highly attenuated, isolated folds are also a common feature within the matrix. The upper part of the matrix-supported conglomerate is typically more clast-rich than the lower portion. Occasionally, at the very top of these beds, planar lamination is evident in muds (and on rare occasions, in very fine sand). Matrix-supported conglomerates are frequently associated with graded beds, and occasionally slumps.

Interpretation: Matrix-supported conglomerates are interpreted to have been deposited through the 'freezing' of cohesive debris flows, making these deposits debrites (e.g. Lowe, 1982; Mulder & Alexander, 2001). The clast-rich matrix with bed-tops of planar laminated mud and very fine sand are indicative of laminar intermediate strength cohesive debris flows (e.g. Talling, 2013). The basal section to these debrites is comparatively clast-poor, suggesting buoyant sorting of individual clasts and blocks within the flow. The clasts of laminated clay and silt may have been incorporated into the flow through substrate delamination (e.g. Fonnesu et al., 2016). It is possible that these mass flows initiated as slope collapse before transitioning downslope into more cohesive debris flows downslope, prior to 'freezing' on the basin floor when the forward momentum dissipated abruptly (Lowe, 1982; Mulder & Alexander, 2001; Sohn, 2000). Matrix-supported conglomerates are frequently overlain by graded beds, suggesting that debris flows were either initiated and deposited first, followed by turbidity currents, or they were cogenetic and part of the same event bed, for instance, the turbidity current forming through dilution and mixing of the upper portion of the debris flow (e.g. Talling et al., 2004).

4.4.3 | Bipartite sand-conglomerate beds (BSC)

Bipartite sand-conglomerate beds are up to 30 cm thick, are relatively rare, and are often associated with MSC beds. They have a sharp basal contact and comprise a lower sand interval and an upper matrix-supported conglomerate interval, with a typical thickness ratio of 1:2 (Figure 9c). The basal interval of well-sorted, normally graded sand is generally structureless with occasional dish structures or parallel laminations. The upper matrix-supported conglomerate interval typically contains lens-shaped mud intraclasts, which can appear aligned and/or folded into tight to isoclinal recumbent folds. Towards the top of the conglomerates, clasts become more rounded to tear-drop shaped, and there is less evidence of folding. The bed tops occasionally consist of planar laminated, very-fine sand.

Interpretation: These bipartite sand-conglomerate beds display traits associated with transitional flow deposits (e.g. Fonnesu et al., 2016; Kane & Ponten, 2012). The lower structureless sand interval containing dish structures signifies rapid deposition and de-watering of sediments from low concentration turbulence-supressed flows (e.g. Lowe, 1982). In contrast, the overlying matrix-supported conglomerate interval represents sediment transported under cohesive flow conditions, as indicated by an abundance of clasts within a mud matrix (Talling, 2013). These beds were deposited by a single flow event, and may either record a cohesive debris flow that has, through mixing with ambient water, begun to transform into a sediment-driven particulate flow (e.g. Mulder & Alexander, 2001), or a turbulent sediment gravity flow that has become more laminar and cohesive due to entrainment of muddy sediments through substrate delamination (e.g. Fonnesu et al., 2016;

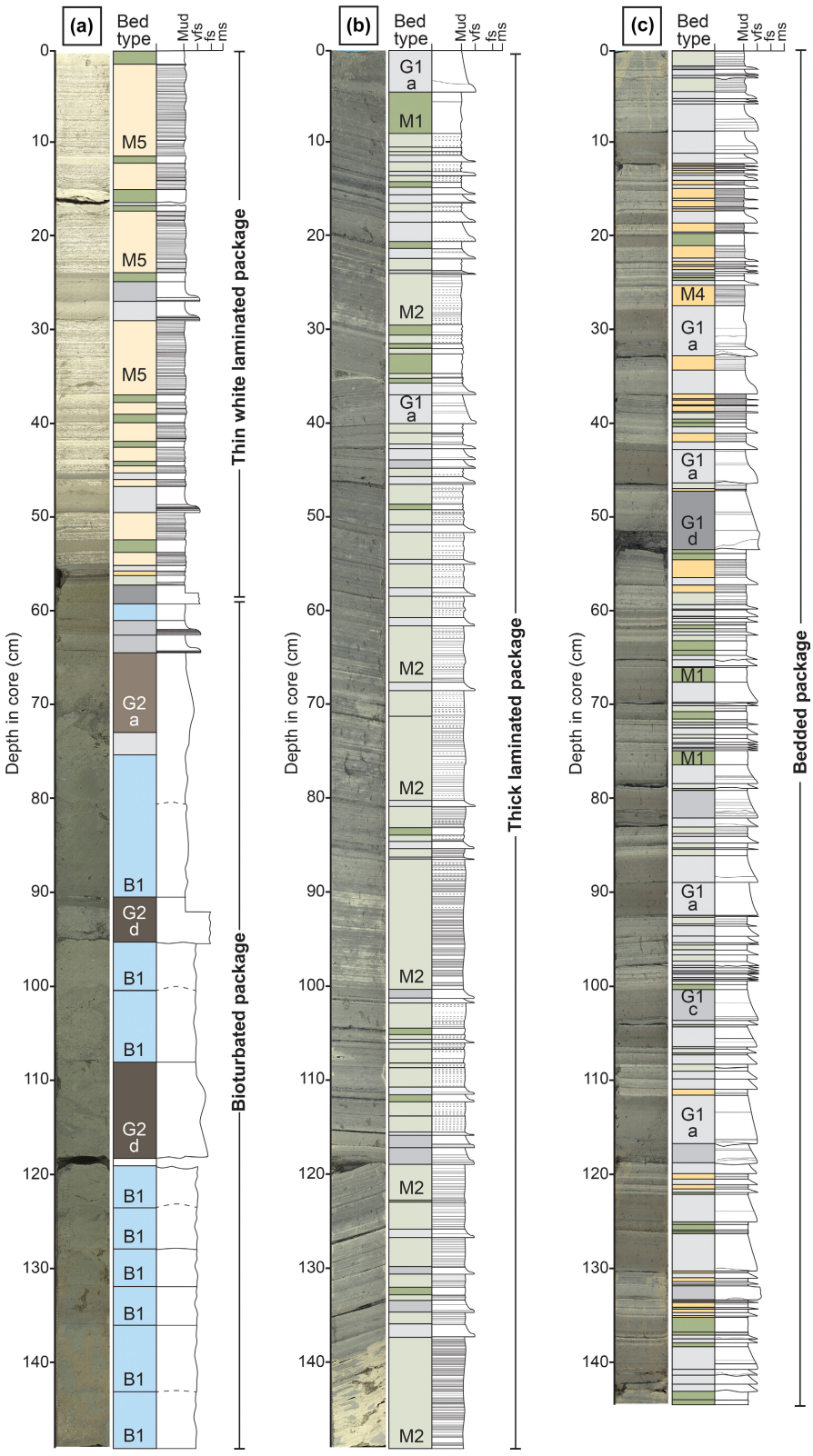

FIGURE 10 Core photographs showing examples of the stratal packages recognised in Lithostratigraphic unit 1, at site M0079 and site M0078. (a) Bioturbated package (site M0079, Core 45R-2, core depth 56–145 cm, borehole depth 167.37–168.26 mbsf) overlain by a thin white laminated package (site M0079, Core 45R-2, core depth 0–56 cm, borehole depth 166.81–168.31 mbsf). (b) Thick laminated package (site M0078, Core 116R-1, core depth 0–145 cm, borehole depth 343.50–345.00 mbsf). (c) Bedded package (site M0079, Core 62R-3, core depth 0–145 cm, borehole depth 242.30–243.75 mbsf). Colour codes refer to bed types in Figure 5

Kane & Ponten, 2012). The close association of MSC and BSC beds suggests that they may have been initiated during the same phase, or phases, of slope destabilisation. As such, the two may be genetically related, with the transitional flow deposits representing a more fluid-rich form of flow compared with the cohesive debris flow deposits.

5 | SYN-RIFT BASINAL STRATIGRAPHY

Based on systematic variations in the stratigraphic distribution of the various mud (M1 to M5) and bioturbated mud (B1) bed types, we recognise three main types of

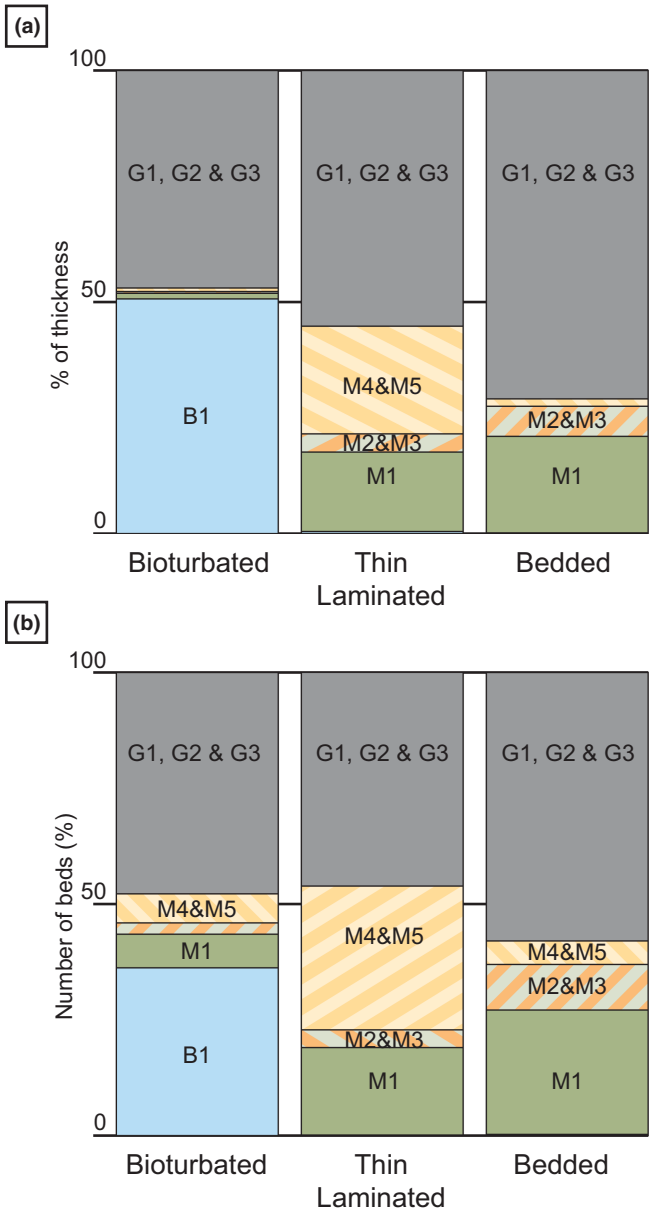

FIGURE 11 Distribution of bed types in the bioturbated, thin white laminated, and bedded packages. (a) Percentage of thickness of each bed type. (b) Number of beds of each bed type

stratal packages in Lithostratigraphic Unit 1 penetrated at sites M0078 and M0079: (i) bioturbated, (ii) laminated, and (iii) bedded (Figures 10 and 11). All package types contain graded beds. The characteristics of these stratal packages are described in the following section. Bed type proportions were established from our detailed logging of the upper 307 m of the succession at Site M0079 (Figure 11), whereas the thicknesses of the packages are based on our analysis of the whole of Lithostratigraphic Unit 1 at both sites M0078 and M0079.

Correlation of the main stratal packages between sites M0078 and M0079 is illustrated in Figure 12. Correlation of the stratal packages is based on identification of the bioturbated packages containing marine microfauna, the abrupt boundaries of the bioturbated packages, and the distinctive occurrence of thin, laminated packages, containing M4 and M5 white laminated beds, at the boundaries of the bioturbated packages. Although there are thickness variations between the two boreholes, the stratigraphic distribution of the stratal packages is markedly similar in M0079 and M0078, which together with the short distance between the boreholes (<6 km) gives us a high degree of confidence in the correlation of the stratal packages illustrated in Figure 12.

5.1 | Bioturbated packages

Bioturbated packages (Figure 10a) form distinctive moderately to extensively bioturbated greenish grey mud-dominated intervals that contain benthic and planktonic microfossil assemblages (McNeill, Shillington, Carter, & Expedition 381 Participants, 2019; McNeill, Shillington, Carter, Everest, et al., 2019) and scattered visible shell debris. They have an average thickness of 12 m, ranging from 5 to 30 m. Bioturbated packages are dominated by bioturbated beds (B1) that comprise on average 50% of the package thickness, and have an average bed thickness of ca. 8 cm. The B1 bioturbated beds are interbedded with thin to very thinly bedded graded beds (G1, G2), that comprise ca. 25% of a bioturbated package and have an average thickness of 3 cm, and with oversized graded beds (G3; i.e. >25 cm thick), which typically form 21% of a package. Very thin beds of homogeneous mud (M1) and white laminated beds (M4, M5) also occur in bioturbated packages, but are rare, forming ca. 1% of each packages. Due to the generally high degree of bioturbation (BI = 4 to 6), bed boundaries and bed types are often difficult to recognise within the bioturbated packages.

Bioturbated packages have abrupt upper and lower contacts and are usually underlain and overlain by thin white laminated packages characterised by M4 and M5 beds (e.g. Figure 10a). Lower contacts of bioturbated packages are characterised by a sudden upward loss of lamination and an abrupt increase in the intensity of bioturbation and change in bed type from finely laminated beds below (M4 and M5) to greenish grey bioturbated beds (B1) within the bioturbated package. Upper contacts are marked by an abrupt loss of bioturbation and a corresponding sudden appearance of parallel lamination and bedding (Figure 10a). Due to the abundance of marine microfossils and the intense degree of bioturbation, bioturbated packages are interpreted to have formed in a marine environment with well oxygenated of bottom waters, requiring a connection between the Gulf of Corinth and the global ocean.

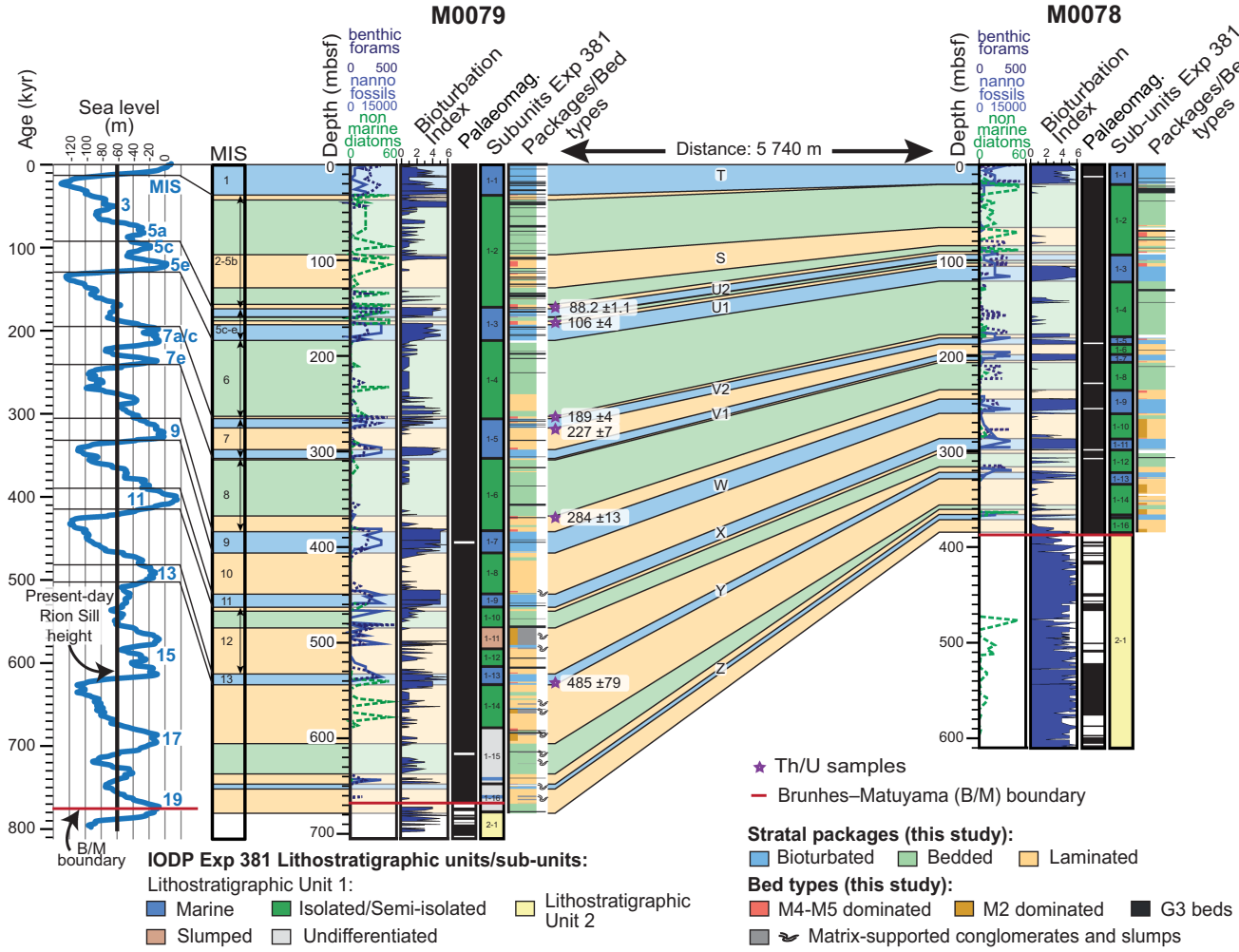

FIGURE 12 Stratigraphic correlation of stratal packages and selected bed types within Lithostratigraphic Unit 1 between sites M0079 and M0078 and interpretated correlation with eustatic sea-level (after Spratt & Lisiecki, 2015) and marine isotope stages (MIS). Location aragonite laminae samples and Th/U isotope ages from site M0079 are shown with purple stars. Abundance/counts of calcareous nannofossils (light blue), benthic foraminifera (dark blue, dotted) and non-marine diatoms (green, dashed), bioturbation index, paleomagnetic results and IODP 381 lithostratigraphic subunits for each site are from Shillington et al. (2019) and McNeill, Shillington, Carter, and Expedition 381 Participants (2019). Lettered bioturbated packages (T, U, V etc.) are discussed in the text

5.2 | Laminated packages

Laminated packages are characterised by mud beds with sub-millimetre to millimetre-thick laminations (M2 to M5) interbedded with homogeneous mud beds (M1) and graded beds. Two types of laminated package occur that have distinctive stratigraphic distribution and thicknesses: (i) thin, typically <5 m thick, laminated packages characterised by well-developed white laminated beds (M4 and M5, Figure 10a) that usually occur adjacent to bioturbated packages, and (ii) thicker laminated packages, averaging 25 m thick, of moderately to well laminated mud (M2), that form the dominant package type in the lower half of Lithostratigraphic Unit 1, and within which the white laminations of M4 and M5 beds are absent or only poorly developed (Figure 10b).

5.2.1 | Thin white laminated packages

The thin white laminated packages typically range in thickness from a few tens of centimetres to 5.5 m. Their striking visual character is due to the distinctive varve-like white laminations of M4 and particularly M5 beds (Figure 8a). Although individual M4 or M5 beds are usually only ca. 1 cm thick, they combine to form on average 23% of package thickness, and may be >50% in some of the thinner packages (Figure 8a).

These thin white laminated packages are typically found immediately above and below bioturbated packages (e.g. Figure 10a). Where they overlie a bioturbated package, the basal few centimetres of the laminated package comprise green laminations, similar in colour to the green mud that dominates the underlying bioturbated package. Where they

are beneath a bioturbated package, the top few centimetres of white lamination can be disrupted and, in some cases, destroyed by a low diversity, but high abundance ichnofauna, for example dominated by *Teichichnus*. Beneath bedded packages, the top few centimetres of laminated beds may display a change from the characteristic pin-stripe white lamination to alternating grey (M2) or black laminations (M3).

The M4 and M5 beds are interbedded with centimetre thick homogeneous mud beds (M1) comprising an average of 17% of the package, and graded beds (G1, G2) that are on average 1.6 cm thick and comprise 47% of the package thickness. Other bed types present are rare and include black laminated beds (M3; average <1% of the package), and oversized graded beds (G3). If present, G3 beds can dominate the thickness of a thin white laminated package because of their large thickness.

5.2.2 | Thick laminated packages

Thick laminated packages mainly occur in the lower half of Lithostratigraphic Unit 1. They are on average 25 m thick, but can be up to ca. 60 m thick. They are much more variable in terms of bed thickness distribution and relative proportions of the different bed types than the thin white laminated packages. Grey laminated beds (M2) are dominant (Figure 10b), whereas the white discontinuous laminated beds (M4) are more sporadically developed, and white laminated beds (M5) are almost entirely absent. Thick laminated packages also contain homogeneous mud beds (M1) and graded beds (G1, G2) (Figure 10b) and, in addition, they also contain matrix-supported conglomerates (MSC) and thick intervals of contorted and sheared bedding (e.g. M0079, 484.48 to 506.40 mbsf; Figure 12).

Both types of laminated package typically lack open marine microfauna, although they locally can contain relatively high abundances of non-marine diatoms and visible shell debris (often gastropods and ostracods). They are therefore interpreted to have been deposited when the Gulf was isolated, or semi-isolated from the global ocean, and basinal waters were non-marine and probably stratified with dysoxic bottom waters. The position of the thin, white laminated packages at the boundaries of the marine bioturbated packages suggest they formed during a transition period between marine conditions when the Gulf had a connection to the global ocean and non-marine conditions when it became isolated from the global ocean.

5.3 | Bedded packages

Bedded packages are mainly composed of graded beds and homogeneous mud beds (M1) (Figure 10c). They have an average thickness of ca. 30 m but may be up to 77 m thick. Graded bed types G1 and G2 are very thinly bedded, averaging only 1.7 cm thick, yet form the dominant component of bedded packages, averaging about 60% of package thickness. Oversized graded beds (G3) account for on average 10% of packages thickness with some individual oversized graded beds exceeding 2 m in thickness (average ca. 1 m). The second main component of bedded packages are homogeneous mud beds (M1), which are typically very thinly bedded (1–2 cm thick) and form, on average, 20% of packages thickness. Laminated beds form <10% of bedded packages thickness, comprising mainly grey laminated beds (M2) and rare discontinuous white thinly laminated beds (M4).

Bedded packages are typically underlain and overlain by laminated packages and are rarely in direct contact with bioturbated packages (Figure 12). Contacts between bedded and laminated packages are relatively abrupt or occur gradationally over several centimetres to a few tens of centimetres, marked by an increase in the presence of grey laminated beds (M2).

Bedded packages are typically devoid of marine microfauna, although some of the graded beds may contain rare occurrences of marine microfauna and shell debris, most likely due to erosion and reworking of older bioturbated packages. We therefore interpret bedded packages to be deposited when the Gulf was isolated, or semi-isolated from the global ocean, basinal waters were non-marine and potentially stratified with a dysoxic basin floor.

5.4 | Stratigraphic variability in Lithostratigraphic Unit 1

Recognition of the three types of stratal packages described above allows a new detailed stratigraphic subdivision of IODP 381 Expedition 381's Lithostratigraphic Unit 1, leading to a new consistent high-resolution correlation of stratal packages between sites M0078 and M0079 (Figure 12). The equivalence between the more detailed stratal packages identified in this study and the original IODP lithostratigraphic sub-units of Shillington et al. (2019) and McNeill, Shillington, Carter, and Expedition 381 Participants (2019), McNeill, Shillington, Carter, Everest, et al. (2019) is shown in Figure 12. Our new work provides a higher resolution breakdown based on bed-scale analysis, both within IODP Expedition 381's marine sub-units (e.g. distinction of marine bioturbated packages separated by bedded and laminated packages), and within the isolated/semi-isolated sub-units (e.g. variability in bedded vs laminated packages and more systematic recognition and classification of major graded beds). The newly identified stratal packages highlight

the consistent occurrence of the thin white laminated packages around the transitions between marine and isolated/semi-isolated sub-units of Lithostratigraphic Unit 1 (Figure 12), which has important implications for changing palaeoenvironment and controls on deposition within the Gulf of Corinth.

Lithostratigraphic Unit 1 is dominated by bedded and laminated packages, interpreted to have been deposited when the Gulf was isolated, or semi-isolated from the global ocean and basinal waters were non-marine. Lithostratigraphic Unit 1 can be divided into two halves based on the thickness and relative importance of bedded and laminated packages. The lower half of the succession in both M0078 and M0079, below 260.70 and 406.02 mbsf respectively, is dominated by thick laminated packages, whereas bedded packages dominate the upper half of the succession (Figure 12). Bioturbated packages, although relatively thin, represent time intervals when the Gulf experienced marine conditions, and occur sporadically throughout Lithostratigraphic Unit 1. Each bioturbated package can be correlated with high confidence between the two boreholes (Figure 12).

The lower half of the succession contains four correlatable bioturbated packages, a very thin bioturbated package (Z; Figure 12) just above the base of Lithostratigraphic Unit 1, and three prominent bioturbated packages (W, X and Y; Figure 12). Bedded packages are relatively rare, and those that are correlated in the lower half of the succession are thin compared to the laminated packages that dominate the lower stratigraphy of Lithostratigraphic Unit 1. Oversized graded beds are sparse in the lower half of Lithostratigraphic Unit 1, however matrix-supported conglomerate and slump deposits are most prominent within the lower half of the succession, compared to the upper half, and are only found in M0079 (Figure 12).

The upper half of Lithostratigraphic Unit 1 is dominated by bedded packages and contains five correlatable bioturbated packages (T, U1, U2, V1 and V2; Figure 12), with the youngest bioturbated package (T on Figure 12) immediately underlying the seafloor. The other four bioturbated packages are arranged into two prominent bioturbated package doublets (U1-U2 and V1-V2; Figure 12). Laminated packages in the upper half of Lithostratigraphic Unit 1, in contrast to the lower half, are predominantly the thin, white laminated packages and systematically occur adjacent to the bioturbated packages (Figure 12). A notable exception is the relatively thick laminated package that occurs in the uppermost part of Lithostratigraphic Unit 1 which is under- and overlain by bedded packages (S; Figure 12). Oversized graded beds are generally more common in this upper half of the succession than the lower half, particularly in the section above the shallowest bioturbated doublet (U1 and U2; Figure 12), and especially in the thicker stratigraphy of M0079 (Figure 12).

5.5 | Fault control on deep basin stratigraphy

Site M0078 is located near the crest of a south-tilted, west-plunging intra-basinal horst (Figure 2a), whereas Site M0079, 5.7 km to the WNW, is located along-strike and down-plunge from the crest of the horst, at a location where the horst has little structural expression (Figure 2b). The horst has minimal bathymetric expression on the present-day basin floor, which is essentially flat with gradients <0.5°. Around Site M0078, thickening occurs into the immediate hanging walls of the faults bounding the horst, and fault offsets extend to the seafloor (Figure 2a). Strata within the lower part of Lithostratigraphic Unit 1 are highly tilted to the south on the horst, they thin and onlap onto the footwall crest of the fault bounding the northern side of the horst. There is a marked expansion of stratigraphy in this fault's hanging wall (Figure 2a). In contrast, in the immediate vicinity of Site M0079 equivalent strata are relatively flat lying with subtle thickening into low amplitude growth synclines in the youngest beds above blind faults at depth (Figure 2b).

Although the present-day bathymetric expression of the M0078 horst is minimal, we ascribe the thinning of the stratal packages between sites M0079 and M0078 (Figure 12) to displacement variations along and between the horst-bounding-faults, with greatest displacement in the east on the fault bounding the northern side of the horst, close to Site M0078. Graded beds are both thicker and more abundant at Site M0079 where there is a relative bathymetric low compared to Site M0078. This variability is exemplified by the difference in frequency and thickness of the oversized graded beds in the upper part of the succession in M0079 (Figure 12).

The more pronounced thinning, onlap and angular differences between the packages in the lower part of the succession imaged on seismic profiles and particularly around Site M0078 corresponds to stratigraphic variations seen on the correlation panel on Figure 12. Both seismic and borehole datasets suggest that the faults were active principally during deposition of the lower half of Lithostratigraphic Unit 1 and that the horst may have had a greater bathymetric expression during this period. High local slip rates and steeper slope gradients along surface-breaking faults bounding the horst could have led to increased slope instability, which may also explain why the lower part of the succession at Site M0079 contains a number of slumped horizons and matrix-supported conglomerates, while these are absent in the younger part of the succession in both M0079 and M0078.

6 | DISCUSSION

The bed types and their associations into distinctive stratal packages provide constraints on depositional processes and the stratigraphic evolution of the Gulf of Corinth over the last ca. 800 kyr. We discuss the changing hydrology of the Gulf of Corinth recorded by the three types of stratal packages and integrate their stratigraphic relationships with Th/U isotopic ages to interpret their relationship to global sea level. We use our bed-scale analysis to discuss the sedimentary processes operating in syn-rift basin floor settings. Finally, we discuss the significance of structural highs that define the boundaries between major segments along rifts and rifted margins on the tectono-sedimentary evolution of rift basins.

6.1 | Basin hydrology and sedimentation variability

There are limited published observations of the hydrology of the present-day Gulf of Corinth. Data from Poulos et al. (1996) and Anderson and Carmack (1973) suggest surface waters down to 100–200 m have marked depth variations of temperature and salinity between winter and summer months, but below this depth range waters have relatively constant temperature (13°C) and salinity (38.5‰). During summer months, temperature and salinity within the upper part of the water column are highest at the sea surface. In winter a maximum in both occurs between 125 and 175 m, interpreted to reflect inflow of Ionian Sea water over the Rion Sill (Anderson & Carmack, 1973). Despite the general stratified nature of the water column, bottom waters down to the basin floor at ca. 850 m are oxygenated (dissolved oxygen >2 ml/L). The lack of anoxia at the seafloor is interpreted to be due to convective overturn during late winter to early spring months (Anderson & Carmack, 1973).

These observations of the modern gulf's hydrology help us to understand the hydrology of the gulf during deposition of the three different stratal package types; bioturbated laminated and bedded (Figure 13). Using the present-day basin as an analogy for the hydrology of the gulf during past interglacials when it was marine, it is likely that during deposition of the bioturbated packages the water column was also oxygenated down to the basin floor, due to winter and early spring convective overturning (Figure 13a). Thus, bottom water and surface sediment conditions were suitable for sustaining a relatively diverse infauna capable of intensely bioturbating the near-bottom sediment, homogenising mud and graded beds to create a largely mottled texture lacking primary sedimentary structures, as seen in the bioturbated packages. Only the thickest oversized graded beds preserve some primary depositional structures, as presumably the rapid deposition of a thick bed exceeded the tiering depth of the ichnotaxa that recolonised the seabed following deposition.

The non-marine bedded and thick laminated packages, are interpreted to have been deposited when the gulf was isolated from global ocean water and became lacustrine. Lowstand shorelines from the last interglacial, imaged in seismic profiles from the Gulf of Corinth (e.g. Leeder et al., 2005; Sakellariou et al., 2007), suggest that, at least for some of the periods when the Gulf of Corinth was isolated from the global ocean, lake level was at the height of the sill. Thus precipitation-to-evaporation ratios were high enough to maintain a lake filled to the spill point of the sill(s) and lake water may have drained across the sills into the ocean (Figure 13b). In the centre of the lake, bioturbation is largely absent and primary sedimentary structures, including sub-millimetre varve-like lamination, are well preserved in bedded and laminated packages. Where rare bioturbation is developed in these packages it is very low in intensity (BI = 1–2), with a monospecific or very low diversity ichnotaxa suggesting a highly stressed environment. Bioturbation is generally only associated with the tops of graded beds, presumably genetically related to emplacement of the graded beds (i.e. flows containing more oxygenated waters). A plausible mechanism for the lack of bioturbation on the basin floor within the bedded and laminated packages is that the gulf's lake water column was strongly stratified, with stable bottom waters that lacked the regular, winter convective overturning to re-oxygenate the deep bottom waters (Figure 13b,c). As a result, bottom waters on the basin floor are interpreted to have been oxygen-depleted, possibly even anoxic at times, creating a highly stressed sea-floor environment hostile to infauna.

A key difference between the bedded and laminated packages is the occurrence of varve-like laminated beds within the latter, suggesting the laminated packages formed during times of pronounced seasonal variability in temperature, surface water salinity, precipitation etc. (Figure 13c). Modern Mediterranean karstic marine-influenced lakes, such as the Mljet lakes in Croatia provide an analogue for the thin white laminated packages in the gulf that mark the transition between marine and lacustrine conditions. The Mljet lakes are flooded karst depressions a few tens of metres deep with a channel connecting them to the open ocean that during late spring and early summer experience whitings that contain high concentrations of suspended needle-like, Sr-rich aragonite crystals (Sondi & Juracic, 2010). Cores of lake floor sediments reveal varve-like laminated sediments comprising alternating white (aragonite) and

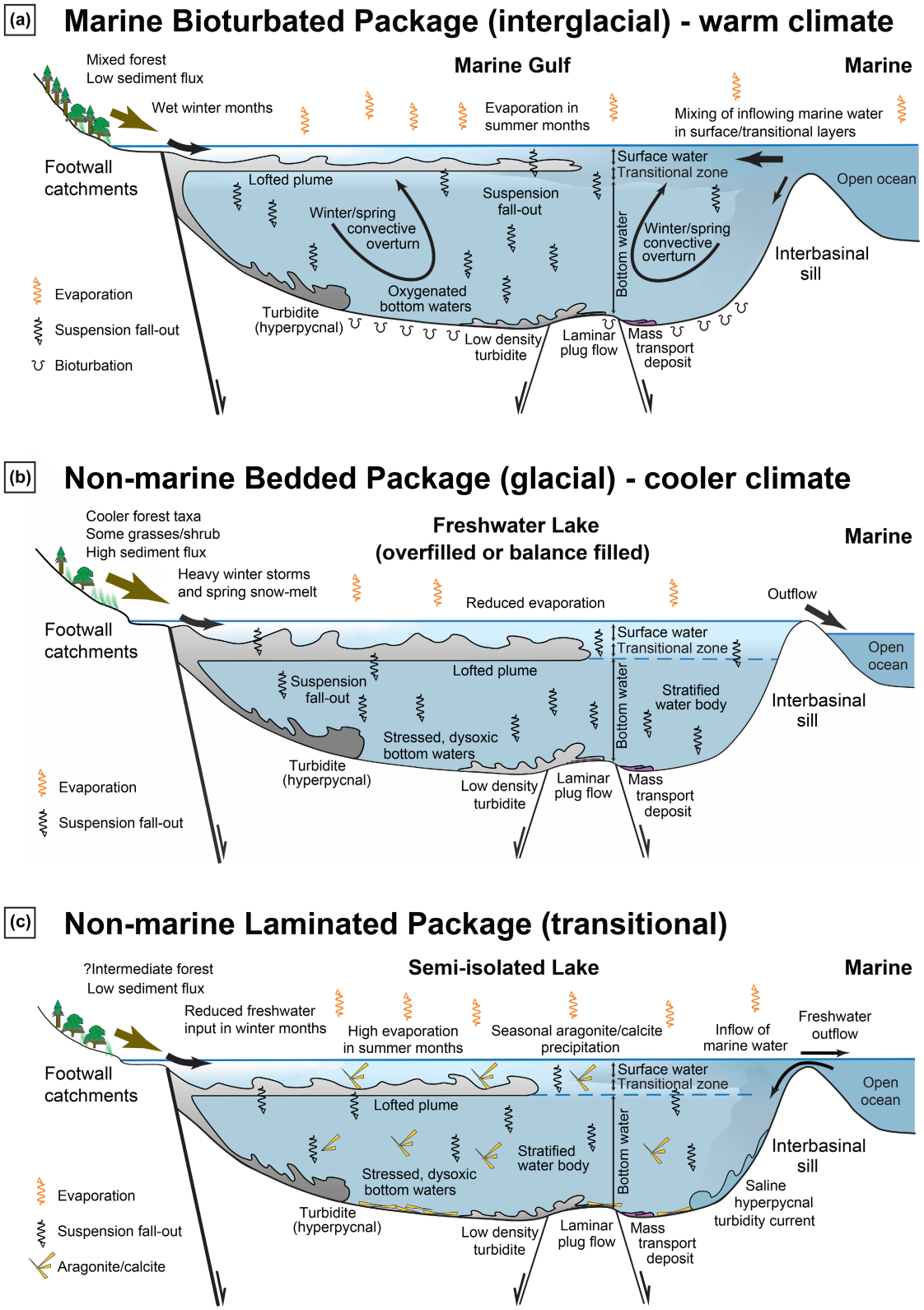

FIGURE 13 Schematic cross sections summarising the sedimentological and hydrological interpretations for the Gulf of Corinth for the three types of stratal package. (a) Bioturbated package deposition during interglacial periods when the gulf was marine, (b) bedded package deposition during glacial periods when the gulf was isolated from the global ocean and was a lake, and (c) laminated package (particularly the thin white laminated packages) deposition during the transitions between glacial and interglacial periods when the gulf was a semi-isolated lake. See text for discussion

TABLE 1 Activity ratios and age calculations from samples of aragonite obtained from Site M0079

Sample (core and core depth)	Depth (mbsf)	$^{234}U/^{238}U$	$^{230}Th/^{238}U$	$^{230}Th/^{232}Th$	Age (ka)
41R-2, 25–27 cm	150.60	1.160 ± 0.007	0.669 ± 0.003	5.3 ± 0.0	88.2 ± 1.1
45R-2, 6–7 cm	166.87	1.224 ± 0.021	0.789 ± 0.012	8.3 ± 0.1	106 ± 4
67R-1, 97.6–98.7 cm	265.28	1.153 ± 0.006	0.995 ± 0.005	2.65 ± 0.01	189 ± 4
69R-1, 136–138 cm	275.62	1.145 ± 0.007	1.043 ± 0.006	3.91 ± 0.02	227 ± 7
88R-3, 11.5–13.5 cm	370.13	1.122 ± 0.007	1.076 ± 0.006	8.50 ± 0.05	284 ± 13
124R-2, 27–29 cm	541.68	1.064 ± 0.006	1.077 ± 0.006	9.48 ± 0.05	485 ± 79

dark (organic matter) laminations (Razum et al., 2021), that are reminiscent of the M4 and M5 white laminated bed types in the IODP 381 cores. The stratigraphic association of the aragonite-rich laminated packages in the Gulf of Corinth at the transition between the alternating marine and lacustrine phases of the gulf's evolution suggest mixing of marine and non-marine waters was significant in the precipitation of the aragonite. Influx of marine waters from adjacent seas over sills into the surface waters of the gulf would increase the Mg/Ca ratio, favouring aragonite precipitation over calcite, and provide a source of Sr. Following the observations from Mediterranean marine-influenced lakes such as the Mljet lakes, Croatia, and Lake Iznik, Turkey (Roeser et al., 2016; Sondi & Juracic, 2010), the aragonite is most likely precipitated in surface waters during late spring and early summer months due to a combination of increased temperature, evaporative concentration of ions and probably a biological trigger (e.g. phytoplankton blooms) (Figure 13c). Once precipitated, aragonite crystals settled through the bottom waters to accumulate on the basin floor several hundred metres below, suggesting bottom waters were not sufficiently undersaturated compared to the settling time of the aragonite crystals to dissolve them. In contrast, during the wetter, cooler winter months aragonite precipitation is not favoured, sediment is mainly composed of detrital grains sourced from river flooding of catchments along the rift margins and deposited by suspension settling or from sediment gravity flows.

The salination of the Corinth water body may have been quite rapid during freshwater to marine transitions, as saline underflows would initially travel as hyperpycnal flows down from the sill, to replace bottom waters, so displacing as well as diluting freshwater upwards and out over the sill (Figure 13c). The prevalence of aragonite/calcite whitings during marine to isolated lake transitions implies that higher Mg/Ca ratios than would be expected for a freshwater lake persisted in the semi-isolated basin at relatively shallow water depths (where precipitation is thought to occur), whilst marine salinities were progressively diluted by freshwater input including as hyperpycnal and lofted flows, supported by any recharge from short-lived marine incursions during this desalination process.

The reduced proportion of graded beds (by number) in laminated packages compared to bedded or bioturbated packages (Figure 11b) supports the suggestion that these phases of deposition occurred during relatively arid phases (at least seasonally arid), given both the reduction in the number of density underflows that reached the basin axis and the higher (summer) temperatures required for carbonate precipitation.

6.2 | Stratigraphic evolution of the Gulf of Corinth over the last 800 kyr

Previous seismic stratigraphic studies have interpreted the alternating high amplitude and transparent reflection packages in the Gulf of Corinth to represent phases of marine and lacustrine conditions in the gulf, and have suggested that they are linked to 100 kyr glacio-eustatic Late Quaternary sea level cycles (e.g. Bell et al., 2008, 2009; Leeder et al., 2005; Lykousis et al., 2007; Moretti et al., 2004; Nixon et al., 2016; Sachpazi et al., 2003; Sakellariou et al., 2007; Taylor et al., 2011). Prior to IODP Expedition 381 these alternating palaeoenvironments were only calibrated by shallow cores sampling down to the last ca. 20–30 ka (Collier et al., 2000; Lykousis et al., 2007; Moretti et al., 2004). Results from IODP Expedition 381 (McNeill, Shillington, Carter, &

Expedition 381 Participants, 2019; McNeill, Shillington, Carter, Everest, et al., 2019) confirm that the distinctive, basin-wide alternations of high amplitude and transparent refection packages of Seismic Unit 2 (Figures 2 and 3) equate to marine and lacustrine conditions (isolated/semi-isolated conditions sensu McNeill, Shillington, Carter, & Expedition 381 Participants, 2019; McNeill, Shillington, Carter, Everest, et al., 2019). Core-log seismic integration suggests that high-amplitude reflections marking marine intervals may arise from lithologic contrasts between sediments deposited during marine and isolated conditions and/or the thin white laminated packages that occur between them and which have relatively low densities (McNeill, Shillington, Carter, & Expedition 381 Participants, 2019). Here we use our new high-resolution package sub-division of the Lithostratigraphic Unit 1 stratigraphy to investigate the controls on deep-water syn-rift sedimentology and stratigraphic evolution.

All of the bioturbated packages can be correlated between sites M0078 and M0079 (Figure 12) and contain calcareous nannofossils and foraminifera indicating deposition in a marine environment (McNeill, Shillington, Carter, & Expedition 381 Participants, 2019; McNeill, Shillington, Carter, Everest, et al., 2019). Following previous work on shallow cores (e.g. Collier et al., 2000; Lykousis et al., 2007; Moretti et al., 2004), we interpret the bioturbated packages to form during prominent interglacial sea-level highstands when global sea-level was higher than the sills at the eastern (Corinth Isthmus) and/or western (Rion Strait) ends of the gulf, so that the gulf experienced marine conditions. Our age model is based on published age determinations based on sedimentation rates (e.g. McNeill, Shillington, Carter, & Expedition 381 Participants, 2019; McNeill, Shillington, Carter, Everest, et al., 2019), magnetostratigraphy and relative palaeointensity data (Maffione & Herrero-Bervera, 2022) and our new Th/U isotopic analysis of aragonite within thin white laminated packages (Table 1 and Figure 12). Based on integration of these datasets there is a good correlation between the occurrence of the bioturbated packages and the major interglacial sea-level highstands of Marine Isotope Stages (MISs) 1, 5, 7, 9 and 11 (T, U, V, W and X respectively on Figure 12). In particular, our Th/U ages indicate that the marine bioturbated packages U1 and U2 developed during the MIS 5 interglacial, V1 and V2 developed during MIS7 interglacial, and W developed during the MIS 9 interglacial (Figure 12).

In the lower part of Lithostratigraphic Unit 1, between the bioturbated package interpreted to represent MIS 11 at ca. 400 ka (X; Figure 12) and the Matuyama-Brunhes boundary (773 ka) near the base of Lithostratigraphic Unit 1, there are fewer bioturbated packages than prominent interglacial sea-level highstands associated with MIS 13 to 19 (Figure 12). Within this part of the succession one distinct and correlatable bioturbated package (Y; Figure 12) is most likely associated with the MIS 13 interglacial based on the U/Th age at the base of this bioturbated package. It is uncertain which interglacial highstand correlates with the very thin bioturbated package close to the base of the studied succession (Z; Figure 12). Other thin intervals with marine microfossils occur within this lower part of the succession (McNeill, Shillington, Carter, & Expedition 381 Participants, 2019; McNeill, Shillington, Carter, Everest, et al., 2019; our Figure 12), but these are not associated with distinctive bioturbated packages. Rather, these sporadic occurrences of marine microfossils occur in prominent slumped intervals (e.g. slump interval in M0079; Figure 12), or in graded beds suggesting they are likely to be reworked.

Previous work in the western part of the Corinth Rift suggests that a large fluvial system, sourced from the Mornos drainage catchment (Figure 1) on the northern side of the gulf, and recorded by the Rodini Formation, extended southward across the western end of the Gulf of Corinth and onto the northernmost Peloponnesos before 400 ka (Ford et al., 2016; Gawthorpe et al., 2018; Somerville et al., 2019). The marine connection through the Rion Strait only began to develop when the south dipping Marathias and north dipping Psathopyrgos faults (Figure 1) became active around 400 ka and subsidence rates in their hanging walls outpaced sediment supply from the Mornos catchment causing drowning and northward retreat of the Rodini fluvial system. Thus, prior to 400 ka, any marine connection to the open ocean must have been in the east, through what is now the Corinth Isthmus (Collier & Thompson, 1991). The height of the Isthmus and structural highs further east within the Saronic Gulf thus become key factors influencing the development of marine conditions within the Gulf of Corinth. The lack of bioturbated packages in the lowermost part of Lithostratigraphic Unit 1, older than 400 ka, suggests that the sill(s) controlling any open ocean connection in the east were much shallower than the present-day depth of the Rion Sill (−60 m) thus preventing any significant marine incursion into the gulf during the interglacials associated with MIS 15, 17 and 19 between ca. 580 and 790 ka (see Figure 12).

Our analysis also suggests the height of sills controlling connection to open ocean waters during the last 400 kyr was significantly shallower than the present-day height of the Rion Sill (−60 m). During the last interglacial highstand (MIS 5) a sill height equal to the present height of the Rion Sill (−60 m) would have generated one continuous marine incursion from ca. 70 to 130 ka, encompassing MIS 5a, 5c and 5e sea-level highstands and the intervening

sea-level lowstands of MIS 5b and 5c (Figure 12). Such a scenario would lead to the deposition of a single marine, bioturbated package. However, the data from M0078 and M0079 indicate MIS 5 comprises a pair of marine bioturbated packages (U1 and U2; Figure 12), separated by non-marine laminated and bedded packages. This suggests two distinct phases of marine connection in the gulf during MIS 5, separated by a phase when the gulf was isolated/semi-isolated. Using the Spratt and Lisiecki (2015) sea level stack, a Rion Sill height of ca. −20 to −25 m would generate two marine incursions in the gulf associated with MIS 5c and 5e, corresponding to bioturbated packages U2 and U1 respectively (Figure 12), separated by a phase of non-marine deposition when the sea-level was below sill height during MIS 5d. This interpretation is consistent with the Th/U age of 88.2 ± 1.1 ka immediately overlying the bioturbated package U2 (Figure 12). A corollary of this interpretation is that the MIS 5a highstand was below sill height and is recorded as part of the laminated or bedded packages immediately overlying the U2 bioturbated package (Figure 12).

This interpretation significantly shortens the time interval that marine bioturbated sediments record during the MIS 5 interglacial highstand to an interval of ca. 30 kyr, between ca. 96 and 127 ka, about half the duration that marine sediments would represent given a −60 m sill height. Applying a similar approach to the older interglacial sea-level highstands back to ca. 400 ka (MIS 11) suggests a sill height similar to that which we suggest existed during MIS 5 (ca. −20 to −25 m) is most likely. A deeper sill would generate more and thicker marine bioturbated packages than actually observed. As with the MIS 5 deposits, the shallower sill height significantly shortens the time interval that marine conditions could exist in the gulf during interglacial sea-level highstands compared to that predicted from the present-day sill height of −60 m. Given the onset of faulting on the Marathias and Psathopyrgos faults around 400 ka and their subsequent growth, it is perhaps not surprising that the height of the sill located in the graben between the two faults has progressively deepened since fault inception to its present-day depth of −60 m.

6.3 | Implications for fine-grained basin floor sedimentation

Detailed logging from the continuous IODP Expedition 381 cores suggests a wide range of processes transport and deposit fine-gained sediment in the relatively small, deep-water Corinth Rift. These include hemipelagite deposition out of suspension, but also a variety of low-density turbidity currents and more highly concentrated flow types depositing a high proportion of the mud-dominated sediment on the basin floor. Deposition out of low-density turbidity currents with overall sediment grain concentrations of <25% (Mulder & Alexander, 2001) may occur by continuous accretion at the base of the flow (e.g. Talling et al., 2012), by the repeated collapse of high concentration, near-bed, laminar sheared layers (Sumner et al., 2008), or by abrupt freezing and en-masse collapse of quasi-laminar or laminar flows at higher mud fractions (Baas et al., 2009, 2011; Baas & Best, 2002; Talling et al., 2012). These processes apply to distal flows that have already deposited coarser, sandy fractions in more proximal settings. Turbulence is well developed in the muddy upper parts of both sand-bearing low-density turbidity currents and of high-density turbidity currents (Lowe, 1982; Mulder & Alexander, 2001; Postma, 1986; Talling et al., 2012). If sediment concentration in the basal layer of a high density sandy turbidity current is sufficient, the whole flow takes on a bipartite character, with the basal massive sand or parallel-laminated sand behaving as a non-cohesive debris flow or grain flow under shear (T_A, $T_{B\text{-}2}$, $T_{B\text{-}3}$; Talling et al., 2012), and the upper layer of the flow recording deposition from a low-density turbidity current ($T_{E\text{-}1}$,$T_{E\text{-}2}$) or muddy density flow ($T_{E\text{-}3}$). Tractional sedimentary structures such as parallel laminations ($T_{B\text{-}2}$) may be enhanced at the top of the basal, mobile sandy bed. Bed types G1d, G2d and G3d may be an expression of this near-independence of the lower and upper parts of 'higher density' sandy waning turbidity currents.

At sites M0078 and M0079, close to the deepest part of the basin centre, we do not observe sandy turbidites without an overlying mud interval. This implies that any associated through-going low-density turbidity current upper layer or tail was itself waning and deposited mud at this basin floor location—including waning after any possible reflection off an opposing basin slope, which we cannot discriminate in unstructured muds. A substantial proportion of the observed laminated mud beds (and probably also homogeneous mud and highly bioturbated beds) without sandy bases (much of bed types M1, M2, M3, and B1) are inferred to have been deposited out of distal turbulent underflows that had already deposited coarser-grained material up-dip. Deposition of coarser-grained material may be induced by local, intra-basinal structurally-controlled lows or gradient changes (e.g. Ge et al., 2018; Pohl et al., 2020; Prather, 2003), and some flows may have bypassed more proximal sites of deposition and only decelerated once out onto the basin-floor (after Talling et al., 2007; Stevenson et al., 2015).

The question arises: can we distinguish between the following depositional processes of homogeneous mud beds (M1): (i) suspension fall-out from the water column, (ii) deposition out of waning low-density turbidity

currents, (iii) deceleration and freezing of quasi-laminar or laminar plug flows? This is intrinsically difficult in the absence of mud intraclasts which might provide direct evidence of hybrid event beds formed in cohesive, debris flow-like muddy flows (Haughton et al., 2003, 2009). We make two apparently contradictory points. Firstly, the M1 mud beds penetrated by the boreholes are dominated by clastic carbonate silts, with a low proportion of clay particles. This may have reduced opportunities for clay flocculation and cohesivity of flows, compared to flows in experimental studies (e.g. Baas & Best, 2002: Baas et al., 2011). But, secondly, the absence of mud intraclasts in this rift axis location may indicate that the mud substrate over which distal flows were passing was itself not strongly cohesive because of its carbonate clay and silt composition, so that sediment was easily entrained into an over-riding (initially low-density and turbulent) flow. This increase in mud content combined with run-out up onto a slope such as the back-tilted M0078 horst block may have favoured the formation of high concentration laminar plug flows which then decelerated rapidly to produce the commonly observed M1 homogeneous muds.

We can reasonably expect that, in a spatially restricted depocentre with steep, fault-controlled slopes and limited shelf areas for sediment storage, direct supply of sediment from hinterland catchments by hyperpycnal flows will be significant. Given the complexities of climate variation through the Late Quaternary, sediment flux will have been sensitive to changes in vegetation and sediment availability for transport in the modest catchment areas around the Gulf of Corinth (Pechlivanidou et al., 2019; Watkins et al., 2018). Superimposed upon this variability, the alternation of marine and lacustrine conditions within the Corinth basin imposes changes in water column density and structure that will have modulated the frequency with which seasonal or storm-related river discharge events translated to hyperpycnal turbulent underflows as opposed to hypopycnal sediment plumes. A simple assumption might be that, for a given population of sediment discharge events at a river mouth, a higher proportion of these would result in hyperpycnal flows into a freshwater basin than into a higher density saline, marine basin. Indeed ca. 70% of the sediment thickness in non-marine bedded packages comprise graded turbidite beds (including rare, oversized graded beds, G3; Figure 11). Unfortunately, the loss of original sedimentary structure in B1 muds of the marine bioturbated packages does not allow us to accurately determine the comparative proportion of sediment thickness deposited as turbidites in these bioturbated packages.

What we do see is that sedimentation rates were generally ca. 2–7 times higher during Late Pleistocene lacustrine phases compared to the marine phases (McNeill, Shillington, Carter, Everest, et al., 2019). Of this sediment, ca. 20% was deposited as centimetre-thick M1 homogeneous mud beds. Having inferred a lack of seasonal overturning that might have re-oxygenated deep bottom waters and therefore the presence of a stratified water column, on the basis of the paucity of bioturbation in these phases, we suggest an additional mechanism which may have contributed to the prevalence of M1 facies. Hyperpycnal flows may entrain water and become progressively more dilute during transport down a steep slope, until they become mutually buoyant with the water column, lofting to form sediment-rich clouds which flow out across a pycnocline that may be temperature-controlled (e.g. Gladstone & Pritchard, 2010; Mulder & Alexander, 2001). Proximal deposits may show normal grading and poorly-sorted characteristics of turbidites. Fine-grained distal deposits may be better-sorted and ungraded, accumulated by suspension fall-out; generating centimetric homogeneous beds if lofted plumes were prolonged. Potential run-out distances for lofted plumes may be shorter than for energetic turbidity currents that can travel hundreds of kilometres downdip, but the 10–15 km distances from the Corinth basin coastline to the rift axis means that suspension fall-out from surface or lofted sediment plumes is perfectly reasonable at the borehole locations. The M1 homogeneous mud beds may therefore include significant contributions from both (i) suspension fall-out from lofted sediment plumes, and (ii) from the deceleration of quasi-laminar or laminar plug flows, which may be a characteristic distal behaviour of turbulent underflows in the Corinth depocentre. Lofting and suspension fall-out may also be prevalent in the marine bioturbated packages, but is hidden by the pervasive bioturbation.

As well as the difficulty in deriving flow process from the mud-dominated facies in the rift axis, inferring the up-dip triggering mechanism of turbidity currents and of higher concentration debris flows remains problematic. Density underflows may be triggered by: (i) extended periods of hyperpycnal fluvial discharge some of which may evolve into lofted flows, (ii) shorter-lived, storm-triggered fluvial discharges causing hyperpycnal flows, (iii) slope instability events creating subaqueous landslides or slumps that undergo disaggregation and dilution downslope into debris flows and/or turbulent underflows; some of which may be triggered during storms (Ferentinos et al., 1988), (iv) "seismites", essentially a seismically-triggered subset of (iii), and (v) possible saline inflow into the axis of the basin when sea-level rise over-topped the level of the structural sill. Campos et al. (2013) and De Gelder et al. (2021) explored whether there may be characteristics of homogenite-turbidite couplets that might distinguish earthquake-triggered events from non-earthquake triggered deposits, specifically deposition of the upper homogenous mud component being by prolonged suspension fall-out from an initially-oscillating cloud of suspended sediment. However, as outlined above,

there are multiple combinations of processes which may lead to sediment bypass and deposition of bipartite beds (Stevenson et al., 2015). Even where current reversals are evidenced by opposing current ripples, these are to be expected in a confined deep-water basin axis (e.g. Talling et al., 2007). We would therefore urge caution in the interpretation of the triggering mechanism for any individual turbidite, slump or debris flow in a narrow rift depocentre, as longitudinal flow evolution responding to combinations of flow type, environmental parameters and the bathymetrically complex basin floor can generate a range of non-unique bed characteristics. Nevertheless, we do expect that a proportion of turbulent and higher density underflows will be seismically triggered in such a tectonically active basin as the Corinth Rift.

6.4 | Implications for tectono-sedimentary evolution of rifts

Various studies have highlighted the role that along-strike displacement variations and normal fault segmentation have in hanging wall depocenter development, in controlling access points for major drainage systems to enter the rift, and on the variability of syn-rift stratigraphic architecture (e.g. Gawthorpe et al., 1994; Gawthorpe & Leeder, 2000; Ravnas & Steel, 1998). Furthermore, the growth and linkage of fault segments and associated strain localisation onto major, linked border fault zones has been cited as a major control on the overall stratigraphic evolution of rift basins (e.g. Cowie et al., 2000; Gawthorpe & Leeder, 2000). The results from this study highlight an additional major control on the stratigraphic evolution of rifts—transverse topographic highs crossing the rift that subdivide the rift into structural domains or major segments, variably called rift segment boundaries, transfer zones, or rift accommodation zones (e.g. Gawthorpe & Hurst, 1993; Morley et al., 1990; Younes & McClay, 2002) (Figure 14). These zones are generally topographic highs characterised by low displacement normal faults as opposed to major high displacement normal faults bounding main rift depocentres. Normal fault configuration in these zones can be complex, generating areas of uplift (horsts) and subsidence (graben/half-graben) that control

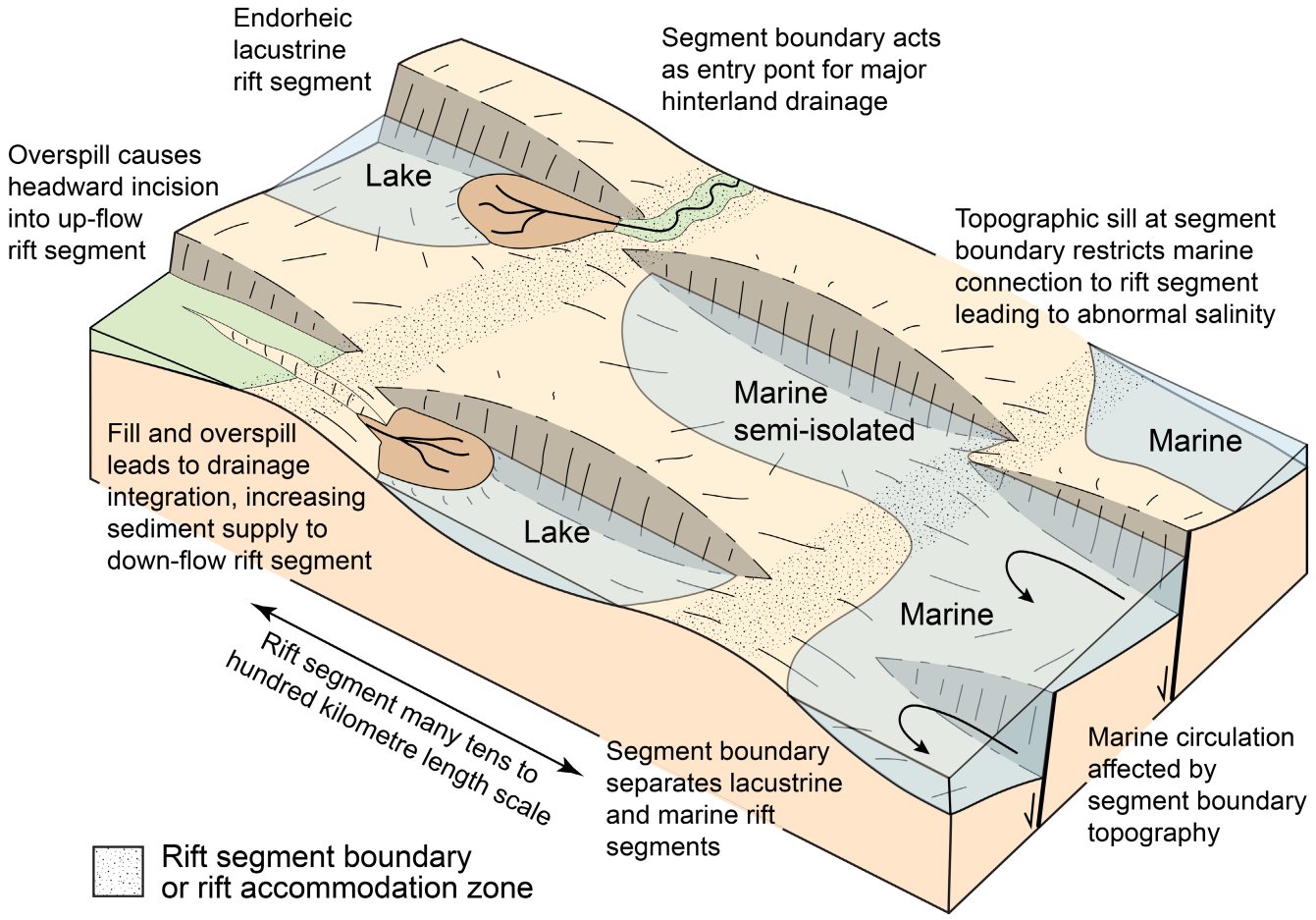

FIGURE 14 Schematic sketch of the varied impact of rift segment boundary structural highs on rift sedimentation in continental (left) to marine (right) settings. See text for discussion

sediment routing along a rift and between rift segments and access to the global ocean (Figure 14).

In the Gulf of Corinth, the Corinth Isthmus at the eastern end, and the Rion Sill at the western end of the rift formed structural highs that have either been above sea-level, or for significant periods have been a few tens of metres lower than present day sea-level. As such, connection to global ocean was controlled by eustatic sea-level variations and the height of these structurally controlled sills. The result is a basin-wide stratigraphic alternation of marine and lacustrine phases, recorded in core by the bioturbated, bedded and laminated packages. Changes in sill elevation may evolve rapidly as seen for example in the closure of the eastern ocean connection by uplift of the Corinth Isthmus, and the opening of the western connection through westward rift propagation, fault initiation and growth causing subsidence of the Rion Sill over the last few hundred thousand years.

Other marine-lacustrine rifts also indicate the importance of rift segment boundaries as sills which controlled connections to global oceans, for example the early Cretaceous of the central South Atlantic rift system (e.g. Chaboureau et al., 2013; Perez-Diaz & Eagles, 2017). During the early rifting stages, deep lacustrine conditions developed within isolated rift segments and episodic marine flooding occurred through seaways at the northern (Tethyan connection) and/or southern (South Atlantic connection) ends of the central South Atlantic rift system. During the late stages of rifting and the transition to ocean spreading in the central South Atlantic, restricted open ocean connections led to the deposition of thick evaporite successions. Similar depositional systems existed in the Suez rift where restricted marine connections at the end of the rift led to deposition of thick evaporites during the Middle-Late Miocene (e.g. Gargani et al., 2008; Orszag-Sperber et al., 1998). These carbonate and evaporite depositional systems provide an arid, low precipitation to evaporation ratio end member for the impact of sills at rift segment boundaries, which contrasts with the more humid, high precipitation to evaporation ratio setting of the Corinth Rift.

Structural highs at ends of rift segments also have an impact in terrestrial rifts without a marine connection. Firstly, they have the potential to control the along-strike extent of lake bodies, and secondly, they have a major impact on axial fluvial systems and drainage integration along the rift (Figure 14). Overspill across rift segment boundaries at spill points is a key control on drainage integration and has a major impact on rift geomorphology and stratigraphic evolution controlling transitions between endorheic and exorheic conditions as illustrated in the Basin and Range province, the Rio Grande Rift and the Central Apennine Rift (e.g. Geurts et al., 2020; Reheis et al., 2014; Repasch et al., 2017).

The example of the Corinth Rift and the other examples of continental and lacustrine-marine rifts discussed here suggest that the structural highs at the ends of rift segments have the potential to be major controls on syn-rift stratigraphic evolution at the rift scale, through their impact on drainage integration and connection to global oceans (Figure 14). The stratigraphy of each rift depocentre then becomes a repository recording semi-independent interactions between local hydrological conditions and local fault evolution, as well as global glacio-eustatic and climatic variations.

7 | CONCLUSIONS

Bed-scale analysis of the last ca. 800 kyr of basin-floor sedimentation in the Corinth Rift at IODP Expedition 381 sites M0078 and M0079 reveal a stratigraphy dominated by distinctive homogeneous and laminated mud beds, highly bioturbated beds, and sharp-based graded beds. In addition, matrix-supported, intraclast-rich conglomerates and slumps form a relatively minor component of the stratigraphy. Based on the relative proportions of mud beds, three types of stratal package have been recognised: bioturbated, bedded and laminated, which are interpreted to reflect different hydrological conditions within the Gulf.

Bioturbated packages are up to a few tens of metres thick, contain marine fauna, and are highly bioturbated (BI = 4–6), such that all but the thickest graded beds are homogenised by bioturbation. They are interpreted to have been deposited during interglacial, sea-level highstands when global sea-level was above the height of structural sills at the eastern and/or western ends of the gulf. As a result, the gulf experienced marine conditions, and the water column was oxygenated down the basin floor due to overturning during winter and spring months. The bedded and laminated packages are generally devoid of marine fauna and bioturbation is mainly absent. This suggests that they were deposited when eustatic sea-level was not sufficiently above sill height to allow significant inflow of marine water, and bottom conditions were dysoxic probably as a result of permanent/semi-permanent stratification of the gulf's water column and lack of seasonal overturning. The abundance of laminated mud within the laminated packages is interpreted to reflect seasonal/annual variation in the gulf's hydrology. In particular, within the thin white laminated packages, varve-like calcite- or aragonite-rich laminations are interpreted to reflect spring summer precipitation of carbonate in near-surface waters and mixing with limited inflow of marine water. The stratigraphic position of these packages, adjacent to the marine, bioturbated packages suggests that they record transitional periods (semi-isolated) between marine and lacustrine (isolated) hydrological conditions within the Gulf.

New Th/U age dates from the aragonite varves confirm interpretations that the basin-wide alternations of marine and lacustrine deposits are driven by eustatic sea-level fluctuations whose impact was moderated by the height of structural sills. The organisation of the bioturbated packages together with age dates in the upper part of Lithostratigraphic Unit 1, suggest sill heights were generally shallower, between −20 to −25 m or less, compared to the present-day height of the Rion Sill (−60 m). As a result, periods of interglacial marine conditions in the gulf were significantly shorter, by up to 50%, than previously estimated using a sill height of −60 m. In the lower part of Lithostratigraphic Unit 1, bioturbated packages are relatively thin and provide an incomplete record of eustatic highstands suggesting even shallower sills, limited interglacial marine connections and prolonged lacustrine phases. The dominance of laminated beds in the lower part of Lithostratigraphic Unit 1 also suggests strong seasonality affecting lake hydrology.

The results of the study indicate a wide range of processes responsible for deposition of mud-dominated sediment in basin floor settings. Characteristics of homogeneous and laminated mud beds imply that mud was transported out onto the basin-floor by varying combinations of (i) suspension fall-out of carbonate precipitates, (ii) hypopycnal plumes and lofted turbidity currents, (iii) low-density turbidity currents that were waning and losing energy 10–15 km from the basin margin, and (iv) quasi-laminar or laminar muddy plug flows developed from basin-floor muds being entrained into these distal underflows. Where muds were deposited in marine and well-oxygenated conditions, they were then intensely bioturbated. Where not destroyed by bioturbation, at least 60%–80% of the succession is deposited from fine-grained sediment gravity flows, the majority of which are mud-dominated and <2 cm thick, rather than hemipelagic deposition. Such a result is perhaps not surprising in a relatively small, enclosed rift basin with limited sediment storage along the sediment routing system.

Our results highlight the importance of structural highs at the ends of rift segments (termed rift accommodation zones or rift segment boundaries) on the overall stratigraphic evolution of rifts. In the Corinth Rift the height of these rift segment boundaries control the influx of marine waters from the global ocean, which in turn drives the basin-wide alternations of marine and lacustrine conditions in the gulf. In more arid marine rifts where rift segment boundaries restrict the connection to the global ocean, significant thicknesses of evaporite deposits may result. In continental rifts, spill across rift segment boundaries have a major impact on drainage integration along a rift and the development of through-going axial drainage connecting rift segments. Current tectono-sedimentary models of rifts stress the role of fault growth and strain localisation as drivers of syn-rift stratigraphic evolution. We suggest that structural highs at rift segment boundaries may also exert a first-order control on syn-rift stratigraphic evolution at the rift scale, with fault segment growth and linkage driving local, intra-rift facies and sequence variability.

ACKNOWLEDGEMENTS

We sincerely thank all involved with the successful completion of IODP Expedition 381, including ECORD Science Operator staff, ship and drilling crew of the D/V Fugro Synergy, and staff at MARUM, University of Bremen. We thank John H (Harri) Wyn Williams for preparing polished thin sections, Irene Heggstad for electron microscopy, Leif-Eric Pedersen, Yuval Ronen and Jenny Maccali for preparation and analysis of aragonite samples for dating. Joe Macquaker and Tom Dodd are thanked for insightful discussions about mud and turbidites respectively. The authors acknowledge support from the Research Council of Norway (DeepRift project; number 308805). RLG thanks the VISTA programme of Norwegian Academy of Science and Letters for the award of the VISTA Professorship which also provided support to SP to participate in IODP Expedition 381 and undertake post-cruise research. RELlC acknowledges NERC for grant NE/S002367/1 for supporting post-cruise research. We thank Peter Burgess for editorial guidance and reviewers Peter Haughton and Bonita Barrett for insightful reviews that improved the manuscript.

PEER REVIEW

The peer review history for this article is available at https://publons.com/publon/10.1111/bre.12671.

DATA AVAILABILITY STATEMENT

The data that support the findings of this study are available from the corresponding author upon reasonable request.

ORCID

Rob L. Gawthorpe https://orcid.org/0000-0002-4352-6366
Natacha Fabregas https://orcid.org/0000-0001-8865-8154
Sofia Pechlivanidou https://orcid.org/0000-0002-0376-6103
Mary Ford https://orcid.org/0000-0002-8343-188X
Richard E. Ll. Collier https://orcid.org/0000-0002-8001-0510
Gareth D. O. Carter https://orcid.org/0000-0002-5994-5565
Lisa C. McNeill https://orcid.org/0000-0002-8689-5882
Donna J. Shillington https://orcid.org/0000-0003-1058-3871

REFERENCES

Alexander, J., Bridge, J. S., Leeder, M. R., Collier, R. E. L., & Gawthorpe, R. L. (1994). Holocene Meander-Belt evolution in an active extensional Basin, southwestern Montana. *SEPM Journal of Sedimentary Research*, *64*(4b), 542–559.

Allen, J. R. L. (1982). *Sedimentary structures: Their character and physical basis*. Elsevier.

Alsop, G. I., & Marco, S. (2013). Seismogenic slump folds formed by gravity-driven tectonics down a negligible subaqueous slope. *Tectonophysics*, *605*, 48–69.

Anderson, J. J., & Carmack, E. C. (1973). Some physical and chemical properties of the Gulf of Corinth. *Estuarine and Coastal Marine Science*, *1*, 195–202.

Armijo, R., Meyer, B., King, G. C. P., Rigo, A., & Papanastassiou, D. (1996). Quaternary evolution of the Corinth rift and its implications for the late Cenozoic evolution of the Aegean. *Geophysical Journal International*, *126*, 11–53.

Avallone, A., Briole, P., Agatza-Balodimou, A. M., Billiris, H., Charade, O., Mitsakaki, C., Nercessian, A., Papazissi, K., Paradissis, D., & Veis, G. (2004). Analysis of eleven years of deformation measured by GPS in the Corinth rift laboratory area. *Comptes Rendus Geoscience*, *336*, 301–311.

Ayranci, K., Harris, N. B., & Dong, T. (2018). Sedimentological and Ichnological characterization of the middle to upper Devonian Horn River group, British Columbia, Canada: Insights into mudstone depositional conditions and processes below storm Wave Base. *Journal of Sedimentary Research*, *88*, 1–23.

Baas, J. H., & Best, J. L. (2002). Turbulence modulation in clay-rich sediment-laden flows and some implications for sediment deposition. *Journal of Sedimentary Research*, *72*, 336–340.

Baas, J. H., Best, J. L., & Peakall, J. (2011). Depositional processes, Bedform development and hybrid bed formation in rapidly decelerated cohesive (mud-sand) sediment flows. *Sedimentology*, *58*, 1953–1987.

Baas, J. H., Best, J. L., Peakall, J., & Wang, M. (2009). A phase diagram for turbulent, transitional, and laminar clay suspension flows. *Journal of Sedimentary Research*, *79*, 162–183.

Backert, N., Ford, M., & Malartre, F. (2010). Architecture and sedimentology of the Kerinitis Gilbert-type fan Delta, Corinth rift, Greece. *Sedimentology*, *57*, 543–586.

Bell, R. E., McNeill, L. C., Bull, J. M., & Henstock, T. J. (2008). Evolution of the Offshore Western Gulf of Corinth. *Geological Society of America Bulletin*, *120*, 156–178.

Bell, R. E., McNeill, L. C., Bull, J. M., Henstock, T. J., Collier, R. E. L., & Leeder, M. R. (2009). Fault architecture, basin structure and evolution of the Gulf of Corinth rift, Central Greece. *Basin Research*, *21*, 824–855.

Bell, R. E., McNeill, L. C., Henstock, T. J., & Bull, J. M. (2011). Comparing extension on multiple time and depth scales in the Corinth rift, Central Greece. *Geophysical Journal International*, *186*, 463–470.

Bernard, P., Lyon-Caen, H., Briole, P., Deschamps, A., Boudin, F., Makropoulos, K., Papadimitriou, P., Lemeille, F., Patau, G., Billiris, H., Paradissis, D., Papazissi, K., Castarede, H., Charade, O., Nercessian, A., Avallone, A., Pacchiani, F., Zahradnik, J., Sacks, S., & Linde, A. (2006). Seismicity, deformation and seismic Hazard in the Western rift of Corinth: New insights from the Corinth rift laboratory (Crl). *Tectonophysics*, *426*, 7–30.

Best, J. I. M., & Bridge, J. (1992). The morphology and dynamics of low amplitude Bedwaves upon upper stage plane beds and the preservation of planar laminae. *Sedimentology*, *39*, 737–752.

Boulesteix, K., Poyatos-More, M., Flint, S. S., Taylor, K. G., Hodgson, D. M., Hasiotis, S. T., & Straub, K. (2019). Transport and deposition of mud in deep-water environments: Processes and stratigraphic implications. *Sedimentology*, *66*, 2894–2925.

Bouma, A. (1962). *Sedimentology of some flysch deposits: A graphic approach to facies interpretation*. Elsevier.

Briole, P., Rigo, A., Lyon-Caen, H., Ruegg, J. C., Papazissi, K., Mitsakaki, C., Balodimou, A., Veis, G., Hatzfeld, D., & Deschamps, A. (2000). Active deformation of the Corinth rift, Greece: Results from repeated global positioning system surveys between 1990 and 1995. *Journal of Geophysical Research: Solid Earth*, *105*, 25605–25625.

Campos, C., Beck, C., Crouzet, C., Carrillo, E., Welden, A. V., & Tripsanas, E. (2013). Late Quaternary Paleoseismic sedimentary archive from deep central gulf of Corinth: Time distribution of inferred earthquake-induced layers. *Annals of Geophysics*, *56*(6), S0670. https://doi.org/10.4401/ag-6226

Chaboureau, A.-C., Guillocheau, F., Robin, C., Rohais, S., Moulin, M., & Aslanian, D. (2013). Paleogeographic evolution of the central segment of the South Atlantic during early cretaceous times: Paleotopographic and geodynamic implications. *Tectonophysics*, *604*, 191–223.

Clarke, P. J., Davies, R. R., England, P. C., Parsons, B., Billiris, H., Paradissis, D., Veis, G., Cross, P. A., Denys, P. H., Ashkenazi, V., Bingley, R., Kahle, H. G., Muller, M. V., & Briole, P. (1998). Crustal strain in Central Greece from repeated Gps measurements in the interval 1989-1997. *Geophysical Journal International*, *135*, 195–214.

Collier, R. E. L., & Dart, C. J. (1991). Neogene to Quaternary rifting, sedimentation and uplift in the Corinth basin, Greece. *Journal of the Geological Society*, *148*, 1049–1065. https://doi.org/10.1144/gsjgs.148.6.1049

Collier, R. E. L., Leeder, M. R., Trout, M., Ferentinos, G., Lyberis, E., & Papatheodorou, G. (2000). High sediment yields and cool, wet winters: Test of last glacial paleoclimates in the northern Mediterranean. *Geology*, *28*, 999–1002.

Collier, R. E. L., & Thompson, J. (1991). Transverse and linear dunes in an upper Pleistocene marine sequence, Corinth Basin, Greece. *Sedimentology*, *38*, 1021–1040.

Cowie, P. A., Attal, M., Tucker, G. E., Whittaker, A. C., Naylor, M., Ganas, A., & Roberts, G. P. (2006). Investigating the surface process response to fault interaction and linkage using a numerical modelling approach. *Basin Research*, *18*, 231–266.

Cowie, P. A., Gupta, S., & Dawers, N. H. (2000). Implications of fault Array evolution for Synrift Depocentre development: Insights from a numerical fault growth model. *Basin Research*, *12*, 241–261.

Cullen, T. M., Collier, R. E. L., Gawthorpe, R. L., Hodgson, D. M., & Barrett, B. J. (2019). Axial and transverse deep-water sediment supply to Syn-rift fault terraces: Insights from the West Xylokastro fault block, gulf of Corinth, Greece. *Basin Research*, *32*, 1105–1139.

Cullen, T. M., Collier, R. E. L., Hodgson, D. M., Gawthorpe, R. L., Kouli, K., Maffione, M., Kranis, H., & Eliassen, G. T. (2021). Deep-water Syn-rift stratigraphy as archives of early-mid Pleistocene Palaeoenvironmental signals and controls on sediment delivery. *Frontiers in Earth Science*, *9*, 715304. https://doi.org/10.3389/feart.2021.715304

Davies, R., England, P., Parsons, B., Billiris, H., Paradissis, D., & Veis, G. (1997). Geodetic strain of Greece in the interval 1892-1992. *Journal of Geophysical Research-Solid Earth*, *102*, 24571–24588.

De Gelder, G., Linh Doan, M., Beck, C., Carlut, J., Seibert, C., Feuillet, N., Carter, G., Pechlivanidou, S., & Gawthorpe, R. L. (2021). Multi-scale and multi-parametric analysis of Late Quaternary event deposits within the active Corinth rift (Greece). *Sedimentology*. https://doi.org/10.1111/sed.12964

Dorsey, R. J., Umhoefer, P. J., & Falk, P. D. (1997). Earthquake clustering inferred from Pliocene Gilbert-type fan deltas in the Loreto Basin, Baja California Sur, Mexico. *Geology*, *25*, 679–682.

Ferentinos, G., Papatheodorou, G., & Collins, M. B. (1988). Sediment transport processes on an active submarine fault escarpment: Gulf of Corinth, Greece. *Marine Geology*, *83*, 43–61.

Fonnesu, M., Patacci, M., Haughton, P. D. W., Felletti, F., & McCaffrey, W. D. (2016). Hybrid event beds generated by local substrate delamination on a Confined-Basin floor. *Journal of Sedimentary Research*, *86*, 929–943.

Ford, M., Hemelsdael, R., Mancini, M., & Palyvos, N. (2016). Rift migration and lateral propagation: Evolution of Normal faults and sediment-routing Systems of the Western Corinth Rift (Greece). *Geological Society, London, Special Publications*, *439*, 131–168.

Ford, M., Rohais, S., Williams, E. A., Bourlange, S., Jousselin, D., Backert, N., & Malartre, F. (2013). Tectono-sedimentary evolution of the Western Corinth rift (Central Greece). *Basin Research*, *25*, 3–25.

Ford, M., Williams, E. A., Malartre, F., & Popescu, S.-M. (2007). Stratigraphic architecture, sedimentology and structure of the Vouraikos Gilbert-type fan Delta, gulf of Corinth, Greece. In G. J. Nichols, E. A. Williams, & C. Paola (Eds.), *Sedimentary processes, environments and basins: A tribute to Peter friend* (Vol. *38*, pp. 49–90). I.A.S. Special Publication.

Gargani, J., Moretti, I., & Letouzey, J. (2008). Evaporite accumulation during the Messinian salinity crisis: The Suez rift case. *Geophysical Research Letters*, *35*(2), L02401.1–L02401.6. https://doi.org/10.1029/2007GL032494

Gawthorpe, R. L., & Clemmey, H. (1985). Geometry of submarine slides in the Bowland Basin (Dinantian) and their relation to debris flows. *Journal of the Geological Society*, *142*, 555–565.

Gawthorpe, R. L., Fraser, A. J., & Collier, R. E. L. (1994). Sequence stratigraphy in active extensional basins: Implications for the interpretation of Ancient Basin-fills. *Marine and Petroleum Geology*, *11*, 642–658.

Gawthorpe, R. L., & Hurst, J. M. (1993). Transfer zones in extensional basins: Their structural style and influence on drainage development and stratigraphy. *Journal of the Geological Society, London*, *150*, 1137–1152.

Gawthorpe, R. L., & Leeder, M. R. (2000). Tectono-sedimentary evolution of active extensional basins. *Basin Research*, *12*, 195–218.

Gawthorpe, R. L., Leeder, M. R., Kranis, H., Skourtsos, E., Andrews, J. E., Henstra, G. A., Mack, G. H., Muravchik, M., Turner, J. A., & Stamatakis, M. (2018). Tectono-sedimentary evolution of the Plio-Pleistocene Corinth rift, Greece. *Basin Research*, *30*, 448–479.

Ge, Z., Nemec, W., Gawthorpe, R. L., Rotevatn, A., & Hansen, E. W. M. (2018). Response of unconfined turbidity current to relay-ramp topography: Insights from process-based numerical modelling. *Basin Research*, *30*, 321–343.

Geurts, A. H., Whittaker, A. C., Gawthorpe, R. L., & Cowie, P. A. (2020). Transient landscape and stratigraphic responses to drainage integration in the actively extending central Italian Apennines. *Geomorphology*, *353*, 107013. https://doi.org/10.1016/j.geomorph.2019.107013

Gingras, M. K., Maceachern, J. A., & Dashtgard, S. E. (2011). Process ichnology and the elucidation of physico-chemical stress. *Sedimentary Geology*, *237*, 115–134.

Gladstone, C., & Pritchard, D. (2010). Patterns of deposition from experimental turbidity currents with reversing buoyancy. *Sedimentology*, *57*, 53–84.

Hang, T. T., Kato, K., & Wada, H. (2014). Magnetic separation of calcite and aragonite for use in radioactive carbon analysis. *Geochemical Journal*, *48*, 113–119.

Haughton, P., Davis, C., McCaffrey, W., & Barker, S. (2009). Hybrid sediment gravity flow deposits—Classification, origin and significance. *Marine and Petroleum Geology*, *26*, 1900–1918.

Haughton, P. D. W., Barker, S. P., & McCaffrey, W. D. (2003). 'Linked' Debrites in sand-rich Turbidite systems—Origin and significance. *Sedimentology*, *50*, 459–482.

Heezen, B. C., Ewing, M., & Johnson, G. L. (1966). The Gulf of Corinth floor. *Deep Sea Research and Oceanographic Abstracts*, *13*, 381–411.

Hemelsdael, R., Charreau, J., Ford, M., Sekar Proborukmi, M., Malartre, F., Urban, B., & Blard, P.-H. (2021). Tectono-climatic controls of the early rift alluvial succession: Plio-Pleistocene Corinth rift (Greece). *Palaeogeography, Palaeoclimatology, Palaeoecology*, *576*, 110507.

Hemelsdael, R., & Ford, M. (2016). Relay zone evolution: A history of repeated fault propagation and linkage, Central Corinth rift, Greece. *Basin Research*, *28*, 34–56.

Hemelsdael, R., Ford, M., Malartre, F., Gawthorpe, R., & Marzo, M. (2017). Interaction of an antecedent fluvial system with early Normal fault growth: Implications for Syn-rift stratigraphy, Western Corinth rift (Greece). *Sedimentology*, *64*, 1957–1997.

Higgs, B. (1988). Syn-sedimentary structural controls on basin deformation in the Gulf of Corinth, Greece. *Basin Research*, *1*, 155–165.

Kane, I. A., & Ponten, A. S. M. (2012). Submarine transitional flow deposits in the Paleogene Gulf of Mexico. *Geology*, *40*, 1119–1122.

Konitzer, S. F., Davies, S. J., Stephenson, M. H., & Leng, M. J. (2014). Depositional controls on mudstone Lithofacies in a Basinal setting: Implications for the delivery of sedimentary organic matter. *Journal of Sedimentary Research*, *84*, 198–214.

Lambotte, S., Lyon-Caen, H., Bernard, P., Deschamps, A., Patau, G., Nercessian, A., Pacchiani, F., Bourouis, S., Drilleau, M., & Adamova, P. (2014). Reassessment of the rifting process in the Western Corinth rift from relocated seismicity. *Geophysical Journal International*, *197*, 1822–1844.

Lazar, O. R., Bohacs, K. M., Macquaker, J. H. S., Schieber, J., & Demko, T. M. (2015). Capturing key attributes of fine-grained sedimentary rocks in outcrops, cores, and thin sections: Nomenclature and description guidelines. *Journal of Sedimentary Research*, *85*, 230–246.

Leeder, M. R., Portman, C., Andrews, J. E., Collier, R. E. L., Finch, E., Gawthorpe, R. L., McNeill, L. C., Pérez-Arlucea, M., & Rowe, P. (2005). Normal faulting and crustal deformation, Alkyonides gulf and Perachora peninsula, eastern gulf of Corinth rift, Greece. *Journal of the Geological Society*, *162*, 549–561.

Lowe, D. R. (1982). Sediment gravity flows: II depositional models with special reference to the deposits of high-density turbidity currents. *Journal of Sedimentary Research*, *52*, 279–297.

Lykousis, V., Sakellariou, D., Moretti, I., & Kaberi, H. (2007). Late Quaternary Basin evolution of the Gulf of Corinth: Sequence stratigraphy, sedimentation, fault–slip and subsidence rates. *Tectonophysics*, *440*, 29–51.

Lyons, R. P., Scholz, C. A., Buoniconti, M. R., & Martin, M. R. (2011). Late Quaternary stratigraphic analysis of the Lake Malawi rift, East Africa: An integration of drill-core and seismic-reflection data. *Palaeogeography, Palaeoclimatology, Palaeoecology*, *303*, 20–37.

Maffione, M., & Herrero-Bervera, E. (2022). A relative paleointensity (RPI)-calibrated age model for the Corinth syn-rift sequence at IODP Hole M0079A (Gulf of Corinth, Greece). *Frontiers in Earth Science*, *10*, 813958. https://doi.org/10.3389/feart.2022.813958

Martinsen, O. J., & Bakken, B. (1990). Extensional and compressional zones in slumps and slides in the Namurian of county Clare, Ireland. *Journal of the Geological Society*, *147*, 153–164.

McNeill, L. C., Cotterill, C. J., Henstock, T. J., Bull, J. M., Stefatos, A., Collier, R. E. L., Papatheoderou, G., Ferentinos, G., & Hicks, S. E. (2005). Active faulting within the offshore Western Gulf of Corinth, Greece: Implications for models of continental rift deformation. *Geology*, *33*, 241–244.

McNeill, L. C., Shillington, D. J., Carter, G. D. O., Everest, J. D., Gawthorpe, R. L., Miller, C., Phillips, M. P., Collier, R. E. L., Cvetkoska, A., De Gelder, G., Diz, P., Doan, M. L., Ford, M., Geraga, M., Gillespie, J., Hemelsdael, R., Herrero-Bervera, E., Ismaiel, M., Janikian, L., … Green, S. (2019). High-resolution record reveals climate-driven environmental and sedimentary changes in an active rift. *Scientific Reports*, *9*, 3116.

McNeill, L. C., Shillington, D. J., Carter, G. D. O., & Expedition 381 Participants. (2019). *Corinth active rift development*. Proceedings of the International Ocean Discovery Program, 381: College Station, TX (International Ocean Discovery Program).

Moore, D. G. (1961). Submarine slumps. *SEPM Journal of Sedimentary Research*, *31*, 343–357.

Moretti, I., Lykousis, V., Sakellariou, D., Reynaud, J.-Y., Benziane, B., & Prinzhoffer, A. (2004). Sedimentation and subsidence rate in the Gulf of Corinth: What we learn from the Marion Dufresne's long-piston coring. *Comptes Rendus Geoscience*, *336*, 291–299.

Morley, C. K., Nelson, R. A., Patton, T. L., & Munn, S. G. (1990). Transfer zones in the east African rift system and their relevance to hydrocarbon exploration in rifts. *American Association of Petroleum Geologists Bulletin*, *74*, 1234–1253.

Mulder, T., & Alexander, J. (2001). The physical character of subaqueous sedimentary density flows and their deposits. *Sedimentology*, *48*, 269–299.

Newport, S. M., Jerrett, R. M., Taylor, K. G., Hough, E., & Worden, R. H. (2018). Sedimentology and microfacies of a mud-rich slope succession: In the carboniferous Bowland Basin, NW England (UK). *Journal of the Geological Society*, *175*, 247–262.

Nixon, C. W., Mcneill, L. C., Bull, J. M., Bell, R. E., Gawthorpe, R. L., Henstock, T. J., Christodoulou, D., Ford, M., Taylor, B., Sakellariou, D., Ferentinos, G., Papatheodorou, G., Leeder, M. R., Collier, R. E. L. I., Goodliffe, A. M., Sachpazi, M., & Kranis, H. (2016). Rapid spatiotemporal variations in rift structure during development of the Corinth rift, Central Greece. *Tectonics*, *35*, 1225–1248.

Ochoa, J., Wolak, J., & Gardner, M. H. (2013). Recognition criteria for distinguishing between Hemipelagic and pelagic Mudrocks in the characterization of deep-water reservoir heterogeneity. *AAPG Bulletin*, *97*, 1785–1803.

Orszag-Sperber, F., Harwood, G., Kendall, A., & Purser, B. H. (1998). A review of the Evaporites of the Red Sea-Gulf of Suez rift. In B. H. Purser & D. W. J. Bosence (Eds.), *Sedimentation and tectonics in rift basins Red Sea:- Gulf of Aden* (pp. 409–426). Springer.

Pechlivanidou, S., Cowie, P. A., Duclaux, G., Nixon, C. W., Gawthorpe, R. L., & Salles, T. (2019). Tipping the balance: Shifts in sediment production in an active rift setting. *Geology*, *47*, 259–262.

Perez-Diaz, L., & Eagles, G. (2017). South Atlantic Paleobathymetry since early cretaceous. *Scientific Reports*, *7*, 11819.

Pohl, F., Eggenhuisen, J. T., Cartigny, M. J. B., Tilston, M. C., De Leeuw, J., & Hermidas, N. (2020). The influence of a slope break on Turbidite deposits: An experimental investigation. *Marine Geology*, *424*, 106160. https://doi.org/10.1016/j.margeo.2020.106160

Postma, G. (1986). Classification for sediment gravity-flow deposits based on flow conditions during sedimentation. *Geology*, *14*, 291–294.

Poulos, S. E., Collins, M. B., Pattiaratchi, C., Cramp, A., Gull, W., Tsimplis, M., & Papatheodorou, G. (1996). Oceanography and sedimentation in the semi-enclosed, deep-water Gulf of Corinth (Greece). *Marine Geology*, *134*, 213–235.

Prather, B. E. (2003). Controls on reservoir distribution, architecture and stratigraphic trapping in slope settings. *Marine and Petroleum Geology*, *20*, 529–545.

Ravnas, R., & Steel, R. J. (1998). Architecture of Marine Rift-Basin successions. *AAPG Bulletin*, *82*, 110–146.

Razum, I., Bajo, P., Brunovic, D., Ilijanic, N., Hasan, O., Rohl, U., Miko, M. S., & Miko, S. (2021). Past climate variations recorded in needle-like aragonites correlate with organic carbon burial efficiency as revealed by Lake sediments in Croatia. *Scientific Reports*, *11*, 7568.

Reheis, M. C., Adams, K. D., Oviatt, C. G., & Bacon, S. N. (2014). Pluvial Lakes in the Great Basin of the Western United States—A view from the outcrop. *Quaternary Science Reviews*, *97*, 33–57.

Repasch, M., Karlstrom, K., Heizler, M., & Pecha, M. (2017). Birth and evolution of the Rio Grande fluvial system in the past 8 Ma: Progressive downward integration and the influence of tectonics, volcanism, and climate. *Earth-Science Reviews*, *168*, 113–164.

Richter, D., Anagnostou, C., & Lykousis, V. (1993). Aragonite Whitings of Pliocene and Pleistocene age in the area of Corinth. *Bulletin of the Geological Society of Greece*, *28*, 553–562.

Roeser, P., Franz, S. O., Litt, T., & Ariztegui, D. (2016). Aragonite and calcite preservation in sediments from Lake Iznik related to bottom Lake oxygenation and water column depth. *Sedimentology*, *63*, 2253–2277.

Rohais, S., Eschard, R., Ford, M., Guillocheau, F., & Moretti, I. (2007). Stratigraphic architecture of the Plio-Pleistocene infill of the Corinth rift: Implications for its structural evolution. *Tectonophysics*, *440*, 5–28.

Sachpazi, M., Clément, C., Laigle, M., Hirn, A., & Roussos, N. (2003). Rift structure, evolution, and earthquakes in the Gulf of Corinth, from reflection seismic images. *Earth and Planetary Science Letters*, *216*, 243–257.

Sakellariou, D., Lykousis, V., Alexandri, S., Kaberi, H., Rousakis, G., Nomikou, P., Georgiou, P., & Ballas, D. (2007). Faulting, seismic-stratigraphic architecture and Late Quaternary evolution of the Gulf of Alkyonides Basin–East Gulf of Corinth, Central Greece. *Basin Research*, *19*, 273–295.

Schieber, J. (1999). Distribution and deposition of mudstone facies in the upper Devonian Sonyea Group of New York. *Journal of Sedimentary Research*, *69*, 909–925.

Shillington, D. J., McNeill, L. C., Carter, G. D. O., Everest, J. D., Le Ber, E., Collier, R. E. L., Cvetkoska, A., Degelder, G., Diz, P., Doan, M. L., Ford, M., Gawthorpe, R. L., Geraga, M., Gillespie, J., Hemelsdael, R., Herrero-Bervera, E., Ismaiel, M., Janikian, L., Kouli, K., … Zakharova, N. V. (2019). *Expedition 381 preliminary report: Corinth active rift development*. International Ocean Discovery Program.

Skourtsos, E., & Kranis, H. (2009). Structure and evolution of the western Corinth rift, through new field data from the Northern Peloponnesus. *Extending a Continent: Architecture, Rheology and Heat Budget*, *321*, 119–138. https://doi.org/10.1144/sp321.6

Sohn, Y. K. (2000). Depositional processes of submarine debris flows in the Miocene fan deltas, Pohang Basin, se Korea with special reference to flow transformation. *Journal of Sedimentary Research*, *70*, 491–503.

Somerville, D. J. P., Mountney, N. P., Colombera, L., & Collier, R. E. L. (2019). Impact of a pre-existing transverse drainage system on active rift stratigraphy: An example from the Corinth rift, Greece. *Basin Research*, *32*, 764–788.

Sondi, I., & Juracic, M. (2010). Whiting events and the formation of aragonite in Mediterranean karstic Marine Lakes: New evidence on its biologically induced inorganic origin. *Sedimentology*, *57*, 85–95.

Spratt, R. M., & Lisiecki, L. E. (2015). A late Pleistocene Sea level stack. *Climate of the Past Discussions*, *11*, 3699–3728.

Stevenson, C. J., Jackson, C. A. L., Hodgson, D. M., Hubbard, S. M., & Eggenhuisen, J. T. (2015). Deep-water sediment bypass. *Journal of Sedimentary Research*, *85*, 1058–1081.

Sumner, E. J., Amy, L. A., & Talling, P. J. (2008). Deposit structure and processes of sand deposition from decelerating sediment suspensions. *Journal of Sedimentary Research*, *78*, 529–547.

Talling, P. J. (2013). Hybrid submarine flows comprising turbidity current and cohesive debris flow: Deposits, theoretical and experimental analyses, and generalized models. *Geosphere*, *9*, 460–488.

Talling, P. J., Amy, L. A., Wynn, R. B., Blackbourn, G., & Gibson, O. (2007). Evolution of turbidity currents deduced from extensive thin Turbidites: Marnoso Arenacea formation (Miocene), Italian Apennines. *Journal of Sedimentary Research*, *77*, 172–196.

Talling, P. J., Amy, L. A., Wynn, R. B., Peakall, J., & Robinson, M. (2004). Beds comprising Debrite sandwiched within co-genetic Turbidite: Origin and widespread occurrence in distal depositional environments. *Sedimentology*, *51*, 163–194.

Talling, P. J., Masson, D. G., Sumner, E. J., & Malgesini, G. (2012). Subaqueous sediment density flows: Depositional processes and deposit types. *Sedimentology*, *59*, 1937–2003.

Taylor, B., Weiss, J. R., Goodliffe, A. M., Sachpazi, M., Laigle, M., & Hirn, A. (2011). The structures, stratigraphy and evolution of the Gulf of Corinth rift, Greece. *Geophysical Journal International*, *185*, 1189–1219.

Watkins, S. E., Whittaker, A. C., Bell, R. E., McNeill, L. C., Gawthorpe, R. L., Brooke, S. A. S., & Nixon, C. W. (2018). Are landscapes buffered to high-frequency climate change? A comparison of sediment fluxes and depositional volumes in the Corinth rift, Central Greece, over the past 130 K.Y. *GSA Bulletin*, *131*, 372–388.

Whittaker, A. C., Attal, M., & Allen, P. A. (2010). Characterising the origin, nature and fate of sediment exported from catchments perturbed by active tectonics. *Basin Research*, *22*, 809–828.

Younes, A. I., & McClay, K. (2002). Development of accommodation zones in the Gulf of Suez-Red Sea rift, Egypt. *American Association of Petroleum Geologists Bulletin*, *86*, 1003–1026.

SUPPORTING INFORMATION

Additional supporting information may be found in the online version of the article at the publisher's website.

How to cite this article: Gawthorpe, R. L., Fabregas, N., Pechlivanidou, S., Ford, M., Collier, R. E., Carter, G. D., McNeill, L. C., Shillington, D. J. (2022). Late Quaternary mud-dominated, basin-floor sedimentation of the Gulf of Corinth, Greece: Implications for deep-water depositional processes and controls on syn-rift sedimentation. *Basin Research*, *34*, 1567–1600. https://doi.org/10.1111/bre.12671